

Theoretical Description of Structural and Electronic Properties of Organic Photovoltaic Materials

Andriy Zhugayevych^{1,2} and Sergei Tretiak¹

¹Theoretical Division, Los Alamos National Laboratory, Los Alamos, New Mexico 87545; email: serg@lanl.gov

²Skolkovo Institute of Science and Technology, Moscow, Russia 143025

Annu. Rev. Phys. Chem. 2015. 66:305–30

First published online as a Review in Advance on January 12, 2015

The *Annual Review of Physical Chemistry* is online at physchem.annualreviews.org

This article's doi:
10.1146/annurev-physchem-040214-121440

Copyright © 2015 by Annual Reviews.
All rights reserved

Keywords

organic solar cell, polarons in organic semiconductors, exciton and charge carrier transport, power conversion efficiency

Abstract

We review recent progress in the modeling of organic solar cells and photovoltaic materials, as well as discuss the underlying theoretical methods with an emphasis on dynamical electronic processes occurring in organic semiconductors. The key feature of the latter is a strong electron-phonon interaction, making the evolution of electronic and structural degrees of freedom inseparable. We discuss commonly used approaches for first-principles modeling of this evolution, focusing on a multiscale framework based on the Holstein–Peierls Hamiltonian solved via polaron transformation. A challenge for both theoretical and experimental investigations of organic solar cells is the complex multiscale morphology of these devices. Nevertheless, predictive modeling of photovoltaic materials and devices is attainable and is rapidly developing, as reviewed here.

PCE: power conversion efficiency

OPV: organic photovoltaic

1. INTRODUCTION

Over the past decade, organic solar cell technologies have made a significant leap in power conversion efficiency (PCE): from a few percent to a current record of 11%. In 2006, the target efficiency was 10% (1); today, that value is routinely reported, and a new goal is set to 20% (2, 3). The fundamental limit for organic photovoltaic (OPV) efficiency is estimated to be somewhere between 20% and the Shockley–Queisser limit of approximately 30% derived for a single bulk inorganic p-n junction (4). The progress in improving the PCE is driven by two factors: the discovery of new OPV materials and the design and engineering of solar cells as devices. The latter historically had limited help from theoretical investigations. In contrast, structural and electronic properties of organic materials can be thoroughly investigated by theory, allowing for purely theoretical prescreening (5). This theory as well as recent progress in modeling OPV materials are the present review subjects.

Parallel to advances in organic electronics (6), the theoretical modeling of organic semiconductors evolved from a consideration of simple models and basic electronic structure calculations to a more or less comprehensive description, in particular, when modeling organic solar cells (7–11). The situation in the field can be characterized as follows: All possible physical mechanisms are already known, as summarized in an excellent textbook (12); the remaining problem is to determine the dominating phenomena for the desired functionality of a particular material and to provide their accurate and efficient descriptions. The main challenge for both theory and experiment is a complex multiscale morphology of typical photovoltaic devices, limiting the possibilities of complete first-principles theoretical modeling and a thorough experimental characterization of both electronic and structural properties. Therefore, with regard to improving the net efficiency of the device, it is often unclear which property of the material might be further optimized (e.g., to reduce different channels for energy losses) without adverse effects on other parameters. Subsequently, a rational design of organic photovoltaic cells is a complex process that has yet to be fully realized in practical terms.

The review is organized as follows: We start in Section 2 with an analysis of the PCE of organic solar cells as the primary target for the discussed research field. In Sections 3 and 4, we review modern theoretical methods for organic semiconductors with an emphasis on the dynamical processes pertinent to solar cells. Finally, in Section 5, we briefly discuss recent progress in modeling organic solar cells. Out of the scope of the current review are processes occurring beyond the active layer or whose theoretical description is far from reliable and predictive, such as performance degradation and aging. For the same reason, the discussion of energy and charge transport in bulk polymers is rather limited in this review. The **Supplemental Appendix** contains an extended list of references, technical details, and additional figures (follow the **Supplemental Material** link from the Annual Reviews home page at <http://www.annualreviews.org>).

2. ORGANIC SOLAR CELLS AS DEVICES

The architecture of nearly all high-efficiency solution-processable (i.e., potentially inexpensive) organic solar cells is the bulk heterojunction (**Figure 1a**). Here, electron donor [e.g., P3HT (poly-3-hexylthiophene)] and acceptor [e.g., PCBM (phenyl-C₆₁-butyric acid methyl ester)] materials are blended from a solution to form the device's active layer. Sunlight is absorbed mainly by one component (typically a molecular donor) with the generation of strongly bound electron-hole pairs (excitons). The excitons diffuse to the heterojunction, in which they dissociate into electrons and holes, collected at the corresponding electrodes. Two classes of organic semiconductors are currently used for donor and acceptor materials: π -conjugated small molecules and polymers. A representative small molecule used in high-efficiency solar cells (13) is shown in **Figure 1e** (R24)

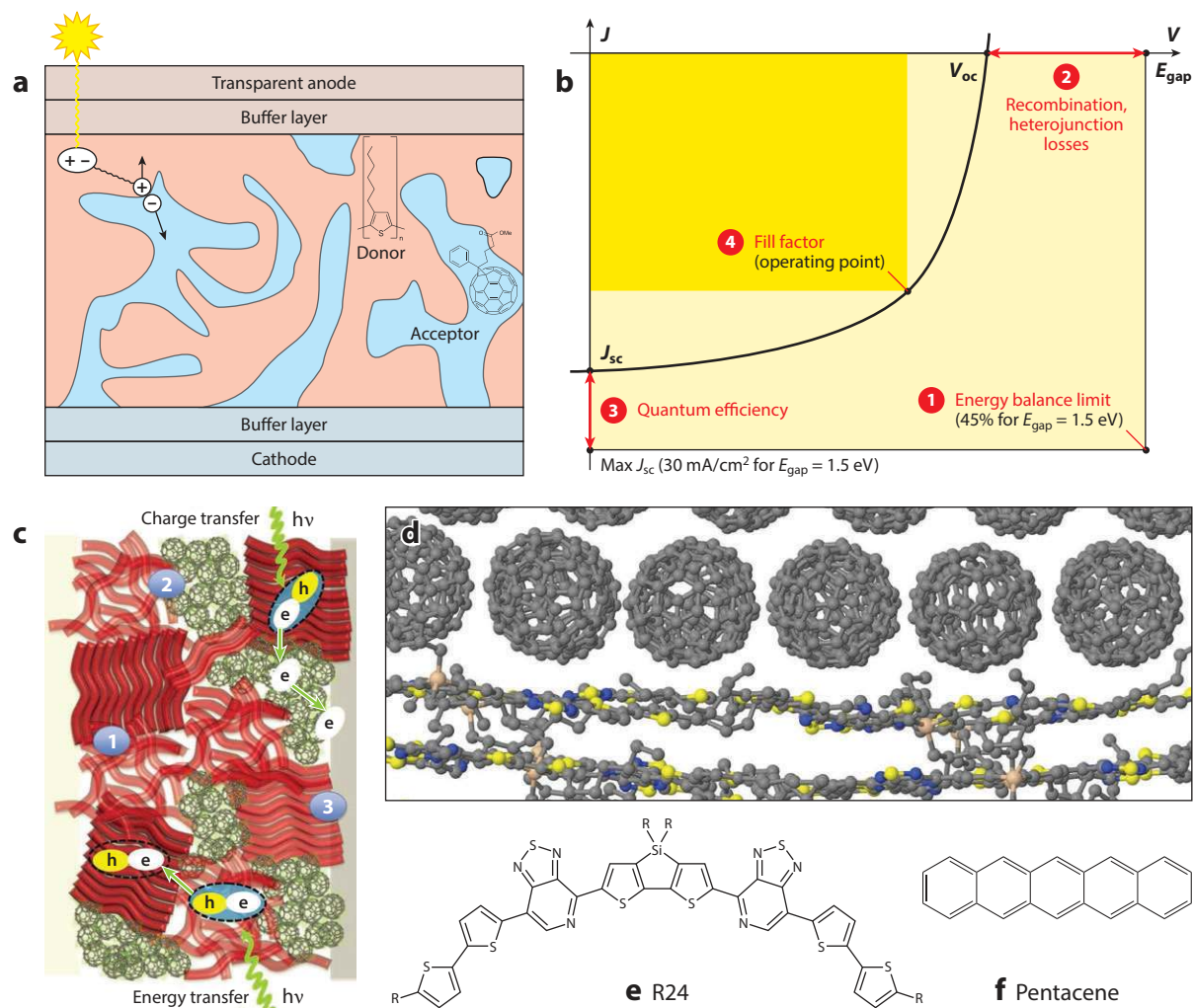


Figure 1

(a) Scheme of a bulk heterojunction organic solar cell, showing the chemical structures of typical donor and acceptor materials [P3HT (poly-3-hexylthiophene) and PCBM (phenyl- C_{60} -butyric acid methyl ester), respectively]. (b) Four factors defining the power conversion efficiency of a solar cell (energy balance limit, recombination and heterojunction losses, quantum efficiency, and fill factor), discussed in Section 2.2. (c) A bulk heterojunction microstructure showing the fundamental charge and energy transfer processes. Numbers 1, 2, and 3 depict the crystalline/amorphous, heterojunction, and organic/semiconductor (or metal) interfaces, respectively. (d) An R24/ C_{60} interface simulated using the classical molecular dynamics approach. (e) The chemical structure of the p -DTS(PTTh) $_2$ = R24 molecule, where DTS, PT, and Th denote dithienosilole, pyridylthiadiazole, and thiophene moieties, respectively. (f) The chemical structure of pentacene.

and is used as an illustrative example throughout the review, together with the thoroughly studied pentacene molecule (Figure 1f).

2.1. Structure and Electronic Processes in the Active Layer

Most of the underlying electronic dynamics occurs in the active layer, whose function is to absorb sunlight and separate charges (Figure 1c). That is why understanding and controlling the

morphology of this layer are important for rational designs of photovoltaic devices (14). When discussing its complex morphology, we need to consider three scales: the structure of the bulk donor and acceptor materials, the microstructure of the interface (**Figure 1d**), and the global macrostructure of the phase separation (**Figure 1a**). The domain size in a bulk heterojunction is limited from above by the exciton diffusion length and from below by the charge separation efficiency, with the optimum size typically a few tens of nanometers. Nucleation agents and other additives are added to control this size (13, 14). New morphologies can be explored based on donor-acceptor molecular frameworks (15) and block copolymers (16).

Upon light absorption, an electronic excitation is created that is delocalized in space and energy. It subsequently relaxes to the lowest excited state, transforming into a Frenkel exciton, which can be localized on a single molecule [the typical case for photovoltaic materials, such as R24 (**Figure 1e**)] or remain delocalized [the case of pure molecular crystals at low temperatures, such as pentacene (**Figure 1f**)] (17). This process of internal conversion takes hundreds of femtoseconds (18, 19). The excitons then diffuse toward a heterojunction. For optimized R24:PCBM blends with a domain size of approximately 20 nm, the estimated diffusion time is of the order of 1 ps if a single-crystal diffusion coefficient (20) is used. The exciton dissociation rates for the interface shown in **Figure 1d** are faster. Traps and geometrical distortions modify the above estimates. Additionally, the direct generation of charge transfer (CT) states in bulk materials and at interfaces is possible (2, 21). Overall, in high-performance organic solar cells, exciton diffusion and dissociation are highly efficient and fast processes, as evidenced by nearly 100% internal photon conversion efficiency (13, 22) and ultrafast pump-probe dynamics (23).

Charge separation is the most intricate process in organic solar cells. In a narrow sense, it is a process of the spatial separation of a geminate electron-hole pair from a CT state at a heterojunction. Timescales and length scales of this process strongly depend on the local geometry and built-in electrostatic field. Typically, the lower limit for the time is of the order of 1 ps, and the upper limit for the spatial separation is approximately 10 nm, as observed within a single polymer chain (24). Thus-generated free charge carriers diffuse or drift toward electrodes within the donor or acceptor material. This process is determined by the global geometry of the active layer and the distribution of charge carrier hopping and recombination parameters (25).

A quantitative simulation of all these electronic processes in a bulk heterojunction is hardly possible. Our understanding of organic solar cell operations is based on modeling individual phenomena in a bulk material or planar interface or using empirical models, as presented below.

2.2. Power Conversion Efficiency Components

In this section, we discuss the main factors determining the PCE to clarify what constituents might be improved. A typical voltage-current curve of a solar cell is shown in **Figure 1b**. The PCE of a photovoltaic cell is usually written as

$$\eta = \frac{J_{sc} \times V_{oc} \times FF}{P_{in}}, \quad (1)$$

where J_{sc} is the short-circuit current, V_{oc} is the open-circuit voltage, FF is the fill factor reflecting the cell's series and shunt resistances, and P_{in} is the incoming radiation flux. The fill factor is the ratio of $J \times V$ at a device operating point (usually the maximum power point) and $J_{sc} \times V_{oc}$. To be able to compare different devices and differentiate the contributions of various factors in the PCE, one can partition the latter into the following product (26):

$$\eta = \eta_{abs}(E_g) \times \frac{eV_{oc}}{E_g} \times \frac{J_{sc}}{J_{sc}^{max}(E_g)} \times FF. \quad (2)$$

Here, the first factor

$$\eta_{\text{abs}}(E_g) = \frac{\int_0^{\lambda_{\text{abs}}} \Phi_{\text{in}}(\lambda) \lambda \, d\lambda}{\int_0^{\infty} \Phi_{\text{in}}(\lambda) \lambda_{\text{abs}} \, d\lambda} \quad (3)$$

is the energy balance limit at which we assume that each photon below the absorption edge $\lambda_{\text{abs}} \equiv 2\pi\hbar c/E_g$ creates an electron-hole pair harvested immediately after the electron and hole relax to the band edges, and Φ_{in} is the spectral density of the incoming radiation ($\text{W}/\text{m}^2/\text{nm}$). The second factor, $eV_{\text{oc}}/E_g < 1$, with e the elementary charge, is the measure of recombination and heterojunction losses (3, 4, 26, 27), reflecting the voltage drop compared to the fundamental gap of the material. Finally, $J_{\text{sc}}/J_{\text{sc}}^{\text{max}}(E_g)$ is an external quantum efficiency, which includes, in particular, optical losses such as transmission and reflection. Here

$$J_{\text{sc}}^{\text{max}}(E_g) = \frac{e}{2\pi\hbar c} \int_0^{\lambda_{\text{abs}}} \Phi_{\text{in}}(\lambda) \lambda \, d\lambda \quad (4)$$

is the maximum short-circuit current, corresponding to one electron generated per every above-band-gap photon. Next we analyze these quantities for organic solar cells by comparing them with inorganic devices (see **Table 1**). The energy balance limit has a maximum of 0.5 for $E_g = 1.1$ eV (when the multiple carrier generation per photon is neglected). Because the band gap of organic materials can be readily tuned, this parameter already attains its maximum value for modern highly efficient organic cells. The next parameter, open-circuit voltage, is the most intriguing because its maximum value is uncertain (3, 4, 26), especially for devices smaller than the incoming light wavelength (28), typical for organic solar cells. The Shockley–Queisser limit for the product of the first two factors, $\eta_{\text{abs}}(E_g)eV_{\text{oc}}/E_g$, is approximately 0.3 (0.4) for nonconcentrated (concentrated) sunlight (29). For the record-breaking GaAs single cell listed in **Table 1**, this value is 0.36 under nonconcentrated sunlight. For highly efficient organic solar cells, the open-circuit voltage approaches that for inorganic cells (**Table 1**). The maximum value of the other two parameters, the quantum efficiency and fill factor, is 1. As for the fill factor, values for OPVs approach those for inorganic cells. In contrast, the quantum efficiency of organic solar cells is rather low. The origin of such a low short-circuit current is mainly from the low absorption efficiency because of the very small thickness of the active layer (100–200 nm) (30). The internal quantum efficiency of organic solar cells (the number of generated electrons per absorbed photon) can exceed 90% on average and approaches 100% at the main absorption band spectral region (22). The problem is that increasing absorption by increasing the active layer thickness results in a decrease in the internal quantum efficiency because charge carriers cannot reach electrodes without losses (14). Increasing the charge carrier mobility and improving the morphology of the active layer for better charge

Table 1 Partitioned power conversion efficiency^a for organic photovoltaic (OPV) and best inorganic solar cells

	OPV (13)	OPV(best) ^b	Si (151)	GaAs (151)
Energy balance limit, $\eta_{\text{abs}}(E_g)$	0.45	0.5	0.49	0.45
Recombination losses, eV_{oc}/E_g	0.5	0.6 (152)	0.63	0.79
Quantum efficiency, $J_{\text{sc}}/J_{\text{sc}}^{\text{max}}(E_g)$	0.5	0.6 (22)	0.97	0.93
Fill factor, $\max JV/J_{\text{sc}}V_{\text{oc}}$	0.6	0.8 (2)	0.83	0.87
Power conversion efficiency	7%	14%	25%	29%

^aThe net power conversion efficiency is a product of four quantities given in the above rows (see Equation 2).

^bOPV(best) refers to the best individual parameters that are not necessarily found in one device. We note that in Reference 22, only 70% of the incoming light is absorbed, so the internal quantum efficiency is 0.9.

transport are among possible solutions of the problem of low quantum efficiency. Additionally, improving light collection has been proposed as an alternative approach (30).

HOMO: highest occupied molecular orbital

LUMO: lowest unoccupied molecular orbital

DFT: density functional theory

3. BASIC STRUCTURAL AND ELECTRONIC PROPERTIES OF ORGANIC SEMICONDUCTORS

The theoretical modeling of OPV materials and devices starts with calculations of basic structural and electronic properties. Among them are the highest occupied and lowest unoccupied molecular orbitals (HOMOs/LUMOs) and excited state energies of a bulk material. The electronic structure of molecular solids is usually a perturbation of the electronic structure of individual molecules in the sense that the individual molecules' one-electron energy levels broadened into bands by intermolecular interactions do not overlap (17, 31). A typical polaron bandwidth at room temperature does not exceed a few tenths of an electron volt; among the largest values is 0.4 eV for pentacene (32). Therefore, the HOMO/LUMO energies of a bulk material can be approximated by the ionization potential and electron affinity of a single molecule in a polarizable medium with some effective dielectric constant. Cyclic voltammetry is the primary experimental technique for validating theoretical approaches (33). Ultraviolet-visible (UV-Vis) absorption spectra of molecular solids may differ in shape from those of monomers in a solution (34), especially at low temperatures. However, the relative positions and intensities of absorption bands corresponding to different electronic transitions are similar for monomers and their ensembles, with a typical shift of the absorption edge within a few tenths of an electron volt (13, 34). Polymers are more complicated for theoretical descriptions, but their electronic structure can be well approximated by oligomers (35). Fully π -conjugated two-dimensional frameworks (15) are even more complicated, but currently they are of limited use in organic electronics.

Typical molecules used in organic electronics include tens to hundreds of atoms. Therefore, density functional theory (DFT) is currently the primary model chemistry approach for these systems. Because of delocalized low-dimensional π -electron systems and strong electron-phonon coupling (35, 36), these molecules are quite challenging for an accurate evaluation of their structural and electronic properties [not mentioning the truly strongly correlated cases (37) irrelevant for photovoltaic applications]. To begin with, reliable wave-function methods, such as the coupled-cluster technique, are computationally tractable only for small molecules rarely used in organic electronics (38). Only the MP2 approach is feasible for the evaluation of some ground state properties of practical-size systems. At the DFT level, however, simple density functionals such as LDA and PBE give highly inaccurate results (39). The most commonly used density functional for small organic molecules is B3LYP combined with the 6-31G* basis set (40). However, for extended π -conjugated systems, B3LYP is unreliable (38, 41, 42), despite its routine use for the geometry optimization and calculation of vibronic couplings for exciton and charge transport. Moreover, B3LYP cannot be used for the description of dispersive intermolecular interactions (43). Recently developed range-separated density functionals including variable fractions of orbital exchange (44, 45), such as CAM-B3LYP, LC- ω PBE, and ω B97X, eliminate the spurious long-range self-repulsion intrinsic to LDA (44) and provide good accuracy for conjugated molecules (38, 39) and their multimers (46). However, current implementations are still imperfect: For non-covalent interactions, empirical dispersion corrections are needed (43); for conjugated molecules, the best-fit range-separation parameter depends strongly on the conjugation length (39), and the methods for ab initio tuning of this parameter are still under development (44, 47).

The use of semiempirical, tight-binding, force field methods is strictly limited to the systems and quantities for which they were parameterized. Among well-parameterized semiempirical methods with conjugated molecules in their training sets is PM7, showing universality and accuracy for

geometries and formation energies (~ 10 kcal/mol). With regard to force fields, a good transferability is expected for MM3 combining a classical force field with a tight-binding description of π -electrons. Other relevant low-cost approaches include self-consistent charge density functional tight binding (48), the molecular mechanics plus Pariser–Parr–Pople (PPP) model for π -electrons (49), and simple tight-binding models (50). Fine-tuning of a force field (51), PPP Hamiltonian (52), or even a density functional (39) is important to increase accuracy and improve reliability.

An important question is whether geometries obtained by such low-cost methods can be used in combination with *ab initio* electronic structure calculations. Here the problem lies in possible artifacts and the inability to describe important effects. For example, the creation of deep traps for charge carriers typically has a large electronic energy penalty, which may not be properly account for by classical force fields. From this point of view, the use of approaches explicitly considering π -electrons has an advantage over a purely classical description.

PES: potential energy surface

4. DYNAMIC ELECTRONIC PROCESSES

An important feature of organic semiconductors is a strong electron-phonon coupling influencing nearly all dynamic processes in these materials (35). For a π -conjugated molecule, there are two distinct kinds of such couplings associated with fast (bond stretching) and slow (librations) molecular motions. The former originates from molecular fragments of alternating single and double bonds (including resonance Lewis structures) (36). In such systems, the HOMO and LUMO are predominantly localized on double and single bonds, respectively, so that HOMO-LUMO excitation or extra charge on these orbitals creates a force trying to revert the pattern of bond length alternation. The latter kind of strong coupling originates from nonrigid dihedral angles across a conjugated system. A planar conformation realizes the maximum π -conjugation along the backbone. With an increase of the dihedral angle, the conjugation strength decreases rapidly. This coupling, for example, propels the femtosecond planarization of oligofluorenes (19) across single bonds and ultrafast photoisomerization across double bonds (53). Additional complexity adds a so-called nonlocal electron-phonon coupling originating from a strong dependence of electron transfer integrals between molecules on an intermolecular geometry (54). Many dynamical phenomena include multiple vibrational and electronic degrees of freedom.

Consequently, a description of such processes as light absorption and energy and charge transport in organic semiconductors must incorporate both electronic and molecular degrees of freedom simultaneously (55). However, first-principles quantum dynamics of all these degrees of freedom (56, 57) is computationally prohibitive even for few-atom molecules. Two basic techniques to overcome this problem are used to treat vibrational degrees of freedom, distinctly employing either a classical description or approximate potential energy surfaces (PESs). In practice, these techniques are usually referred to as nonadiabatic molecular dynamics (NAMD) and the effective Hamiltonian approach, respectively. In this section, we briefly mention the first method, which is detailed in many other reviews (58, 59), and primarily focus on the second one.

Commonly used atomistic NAMD methods are frequently referred to as mixed quantum-classical dynamics treating the slow vibrational (nuclear) motion by classical mechanics, but the forces that govern the classical motion incorporate the influence of nonadiabatic transitions between electronic states (55). In popular surface-hopping approaches, such transitions are considered as stochastic jumps between electronic levels (58). For simulations in organic electronics, the current state-of-the-art NAMD methods still have important fundamental and technical limitations. Fundamentally, they require proper accounting of the interactions between classical and quantum subsystems (55). Computationally, evaluating excited electronic states at each point of the molecular dynamics (MD) trajectory is numerically demanding. For small-scale simulations,

time-dependent DFT can be used, but for the description of intermolecular charge/energy transfer between medium-sized molecules, a simplified quantum chemistry approach is needed, such as a semiempirical (18) or even a tight-binding (59) framework. Moreover, strongly coupled, bond length alternation vibrational modes have high frequencies, of the order of 0.2 eV, so a classical treatment of these modes may introduce systematic errors owing to the lack of tunneling processes and to unphysical energy flow between different vibrational modes due to the inability to describe zero-point energy, for example (60). Alas, approaches correctly describing quantum modes dramatically increase computational demands (61). Finally, an accurate description of decoherence effects during nonadiabatic transitions and interference between them (e.g., in the case of band-like transport) can make NAMD simulations computationally prohibitive for extended systems (62).

4.1. Holstein–Peierls Hamiltonian

In the second approach, we want to be able to treat vibrational modes quantum mechanically at the cost of having simplified PESs. A common approximation is harmonic PESs and linear electron-phonon couplings. If, additionally, a one-particle approximation is assumed for an electronic subsystem, then we obtain the Holstein–Peierls model (63–65), which is the simplest Hamiltonian accounting for strong electron-phonon interactions in organic semiconductors:

$$\sum_{ij} H_{ij}^{\text{lp}} c_i^\dagger c_j + \sum_{\alpha} \hbar\omega_{\alpha} \left(b_{\alpha}^\dagger b_{\alpha} + \frac{1}{2} \right) + \sum_{ij\alpha} \hbar\omega_{\alpha} g_{\alpha ij} (b_{\alpha}^\dagger + b_{\alpha}) c_i^\dagger c_j. \quad (5)$$

Here c_i^\dagger (c_i) and b_{α}^\dagger (b_{α}) are the creation (annihilation) operators for electronic quasi-particles (electrons, holes, or Frenkel excitons) and vibrational normal modes (or phonons and vibrons), respectively; $g_{\alpha ij}$ are dimensionless electron-phonon couplings. The diagonal elements of the one-particle Hamiltonian H^{lp} are called on-site energies, $H_{ii}^{\text{lp}} \equiv \varepsilon_i$; the other elements are transfer integrals, t_{ij} . Similarly, couplings $g_{\alpha ii} \equiv g_{\alpha i}$ are called local; the others are nonlocal. The Hamiltonian with purely local, fully separated ($g_{\alpha i} g_{\alpha j} = 0$ for $i \neq j$) couplings is called a Holstein Hamiltonian. Nonlocal couplings are related to Peierls instability, such as the dimerization of *trans*-polyacetylene (66). For a system consisting of small-enough molecules (including a cluster, crystal, or amorphous solid), the sites can be associated with individual molecules. The essential condition here is for t_{ij} to be small enough compared to the separation between intramolecular energy levels. Otherwise, more than one site (electronic degree of freedom) per molecule is required. The situation with extended systems (e.g., polymers, dendrimers, or frameworks) is more complicated, but a one-particle Hamiltonian can usually be well defined (67). We note that the Hamiltonian in Equation 5 can be considered either as an empirical or first-principles model, depending on whether its parameters are fitted to experimental data or quantum chemistry calculations. Finally, vibrational modes can be rigorously coarse grained with the energy bin of the order of the bath temperature (see Equation 10). Quite often, consideration of only a few modes with strong couplings in Equation 5 suffices.

There are three challenges in using the Holstein–Peierls model. First, despite its visual simplicity, the Hamiltonian in Equation 5 is not exactly solvable. Moreover, no efficient numerical solvers exist for a general case. Second, the approximations under which this Hamiltonian is valid are rarely fully satisfied in organic semiconductors. In other words, Equation 5 is only a minimal model of electronic dynamics in organic materials. Third, in first-principles simulations of real-world materials, it is important to have efficient and reliable schemes for an ab initio evaluation

of the parameters of the Hamiltonian in Equation 5 (H_{ij}^{1p} , ω_α , $g_{ij\alpha}$). In the rest of this subsection, we discuss the last two issues.

There are three intrinsic approximations of the Holstein–Peierls model corresponding to the three terms in Equation 5. First, the electron–electron interaction is treated statically (i.e., in a mean-field fashion). This is acceptable for a bulk material in nonconcentrated-sunlight photovoltaic devices (with the incident solar flux being 5 photons/ns/ μm^2) but may be unacceptable at interfaces in which excitons, electrons, and holes can be accumulated. Next, the harmonic approximation for intramolecular atomic motion is valid only for small rigid molecules, such as pentacene, whereas typical molecules used in photovoltaics have few-to-many highly anharmonic librations (68). Notably, intermolecular motions are highly anharmonic at room temperature because of the close proximity to the melting point. Finally, the linear local electron–phonon coupling approximation gives mirror symmetry for absorption and emission spectra, which is not the case for many conjugated molecules. For nonlocal couplings, the linear approximation is barely acceptable. Of course, any of the above effects can be taken into account by modifying the Hamiltonian in Equation 5, but such generalizations are nontrivial and lie far beyond the scope of the present review.

A first-principles evaluation of the parameters of an effective electronic Hamiltonian is based on the fitting of single-particle and total energies to quantum chemistry calculations, which is a well-elaborated procedure for crystalline inorganic semiconductors (69) and conjugated polymers (70). For molecular solids in organic electronics, simplified approaches are used, except for very small molecules (71). A common scheme is the dimer approximation in which the three quantities, H_{ij}^{1p} , H_{ii}^{1p} , and H_{jj}^{1p} , are estimated from first-principles calculations of the ij dimer in its “ground state” (no quasi-particle present) geometry using molecular orbitals or energies (see 20, and references therein). In addition, simplified approaches exist that require only self-consistent field calculations of monomers (72, 73). A poorly studied issue of the dimer approximation is the influence of other molecules on calculated transfer integrals, such as the solvent screening of exciton transfer at large intermolecular separations (20, 74). The dependence of the calculated transfer integrals on the basis set is inessential (75), whereas the dependence on the density functional is noticeable: Upon an increase of the orbital exchange in the DFT model, transfer integrals can increase by a factor of two (76). Among semiempirical approaches, ZINDO is the only known reliable method for calculating transfer integrals.

The evaluation of local vibronic couplings, $g_{i\alpha}$, is a straightforward procedure with the use of two geometries: the “ground state” and “excited state” (one quasi-particle present). Computations of nonlocal couplings as well as lattice phonons are more elaborate (54, 71, 77). The main challenge here for nonrigid molecules results from the intramolecular–lattice mode mixing, anharmonism, and nonlinear electron–phonon coupling. Another challenge is the strong dependence of vibronic couplings on a computational method including a basis set (20, 78).

A more severe problem may arise with the determination of quasi-particle sites in the Hamiltonian in Equation 5. For molecular systems in which each molecule hosts one adiabatic polaron state (meaning that all other states are separated by an energy gap), the sites are naturally assigned to individual molecules: HOMO for holes, LUMO for electrons, first singlet or triplet excitations (S_1 or T_1) for excitons. For extended molecules such as polymers, this procedure may be nontrivial. If the polymer conjugation length is larger than the polaron size (42), then the polaron wave functions significantly overlap spatially, and intramolecular nondiagonal electron–phonon couplings appear. In the opposite case, the quasi-particle sites are ill-defined because of a strong coupling between an electronic wave function and molecular conformation. In this case, an anharmonic PES must be used (at least for dihedrals) (70). For these reasons, NAMD is currently the best tool for first-principles modeling of polymers (49, 58).

4.2. Mean-Field Polaron Approximation

It is hardly possible to mention all existing approaches in solving the Holstein–Peierls and similar Hamiltonians (63, 79). Among those used in modeling organic semiconductors are the already-mentioned surface-hopping technique (58, 80), direct numerical solution (56, 81), the truncation of boson excitations (34), projected modes (82), and a variational approach (83), as well as various approximations based on the generalized master equation (84). Pertinent to organic semiconductors, the most universal approach with respect to the model parameter space is the mean-field polaron (MFP) approximation (63, 85).

Here, we illustrate the idea of the MFP approach for the Holstein model. The general case in Equation 5 is conceptually the same but is technically more involved (71) (see the **Supplemental Appendix**). The starting point is to apply the polaron transformation (63) to the Holstein Hamiltonian: $\mathbb{H} \rightarrow e^{\mathbb{S}} \mathbb{H} e^{-\mathbb{S}}$, where $\mathbb{S} = \sum_{i\alpha} g_{\alpha i} (\mathbf{b}_{\alpha} - \mathbf{b}_{\alpha}^{\dagger}) \mathbf{n}_i$ and $\mathbf{n}_i = c_i^{\dagger} c_i$. This transformation formally eliminates the electron-phonon interaction term in Equation 5, yielding the polaron Hamiltonian,

$$\mathbb{H}^{\text{polaron}} = \sum_i (\varepsilon_i - \lambda_i) \mathbf{n}_i + \sum_{i \neq j} \left[t_{ij} \prod_{\alpha} \mathbb{D}_{\alpha}(g_{i\alpha} - g_{j\alpha}) \right] c_i^{\dagger} c_j, \quad (6)$$

where

$$\lambda_i = \sum_{\alpha} S_{\alpha i} \hbar \omega_{\alpha} \quad (7)$$

is the polaron relaxation energy, $S_{\alpha i} = g_{\alpha i}^2$ are Huang–Rhys factors, and $\mathbb{D}_{\alpha}(g) = e^{g(\mathbf{b}_{\alpha} - \mathbf{b}_{\alpha}^{\dagger})}$ is the displacement operator, $D(g)\psi(\xi) = \psi(\xi + g)$, whose matrix elements over harmonic oscillator eigenfunctions are Franck–Condon factors. Because these factors are smaller than unity, the transfer integrals are renormalized in the direction of band narrowing.

In the MFP approximation, the displacement operators are substituted by their effective (mean-field) values whenever is needed (it is important to take late averages). For the thermal average over the Boltzmann distribution, the MFP transfer integrals are given by

$$t_{ij}^{\text{polaron}} = t_{ij} \exp \left(- \sum_{\alpha} R_{\alpha ij} \coth \frac{\hbar \omega_{\alpha}}{2T} \right), \quad (8)$$

where $R_{\alpha ij} = (S_{\alpha i} + S_{\alpha j})/2$, and T is a temperature (85).

There are two major problems with the MFP approach. First, as is common for mean-field theories, it is unclear how accurately electron-phonon correlations are treated. Second, in molecular π -conjugated systems, there are slow modes with strong electron-phonon couplings (librations and intermolecular motions), which do not equilibrate during the motion of electronic quasiparticles. A detailed discussion of this and other technical challenges is given in Section S2 of the **Supplemental Appendix**.

4.3. Nature of Electronic States

Because of strong electron-phonon coupling (i.e., intermolecular electronic couplings and polaron relaxation energy are often of comparable magnitudes), charge and excitation carriers in organic semiconductors (quasi-electrons, holes, Frenkel excitons) are polarons, which involve inseparable electronic and molecular degrees of freedom. An adiabatic polaron gives a clear visual picture and straightforward computational protocol for identifying such states (42) (see **Figure 2a**). Despite the lack of a phase transition in the Holstein–Peierls model (79), the physical properties of the polaron are quite different in different regions of the parameter space. In the simplest possible case (one phonon mode per site and zero temperature), this space consists of two dimensionless

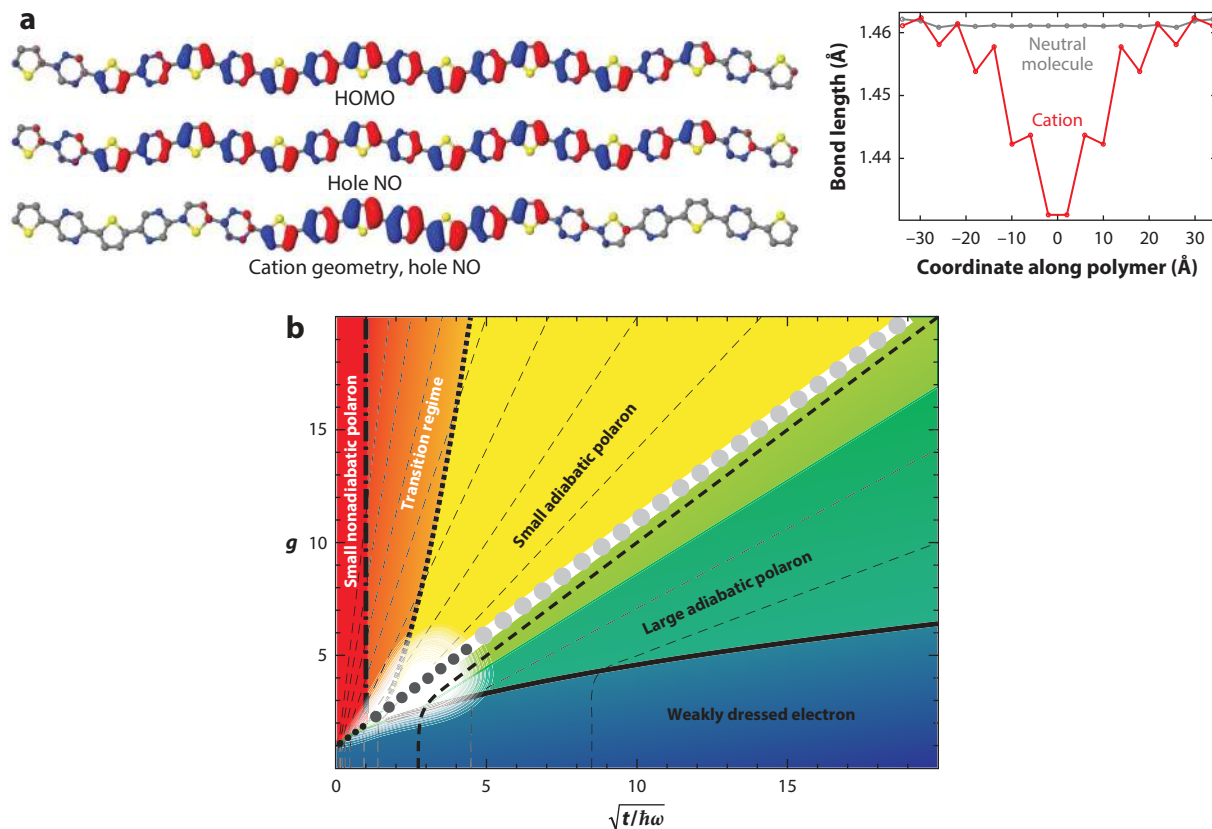


Figure 2

(a) Illustration of an adiabatic hole polaron. Its spatial localization is clearly visible in both the electronic wave function and deformed molecular structure. (b) Parameter space of the one-dimensional Holstein model. Notably, the vibrational modes of the R24 molecule on this diagram cover the entire range of parameter values. Panel b adapted with permission from Reference 150.

parameters: g and $t/\hbar\omega$. Even in this case, there are several contrasting regions in the parameter space (see **Figure 2b**).

The region that is easiest to understand is that of fast vibrational modes, $\hbar\omega \gg t$, corresponding to C–C stretching modes in conjugated molecules. In this case, the polaron is a coherently evolving superposition of electronic and vibrational degrees of freedom, and the MFP approach correctly describes this state for all values of g and T . In particular, the transition from a band-like motion to the hopping regime is caused by the exponential bandwidth reduction and is described by the formula given in Equation 8. Because there is no phase transition in the Holstein–Peierls Hamiltonian itself, the polarons are localized by coupling to environment or static disorder, which is ever present in real systems, when the bandwidth becomes small enough. In the case of C–C stretching modes, the band-narrowing factor is nearly temperature independent (71) and is given by e^{-S} , where S is the total Huang–Rhys factor for these modes. That is why these modes never localize polarons in realistic π -conjugated systems ($\hbar\omega \sim 0.2$ eV, $g \sim 1$) below their thermal decomposition temperature.

At the opposite side of the diagram in **Figure 2b** are slow modes, $\hbar\omega \ll t$. In materials with a charge carrier mobility that is not too small ($t > 50$ meV), lattice modes and librations usually

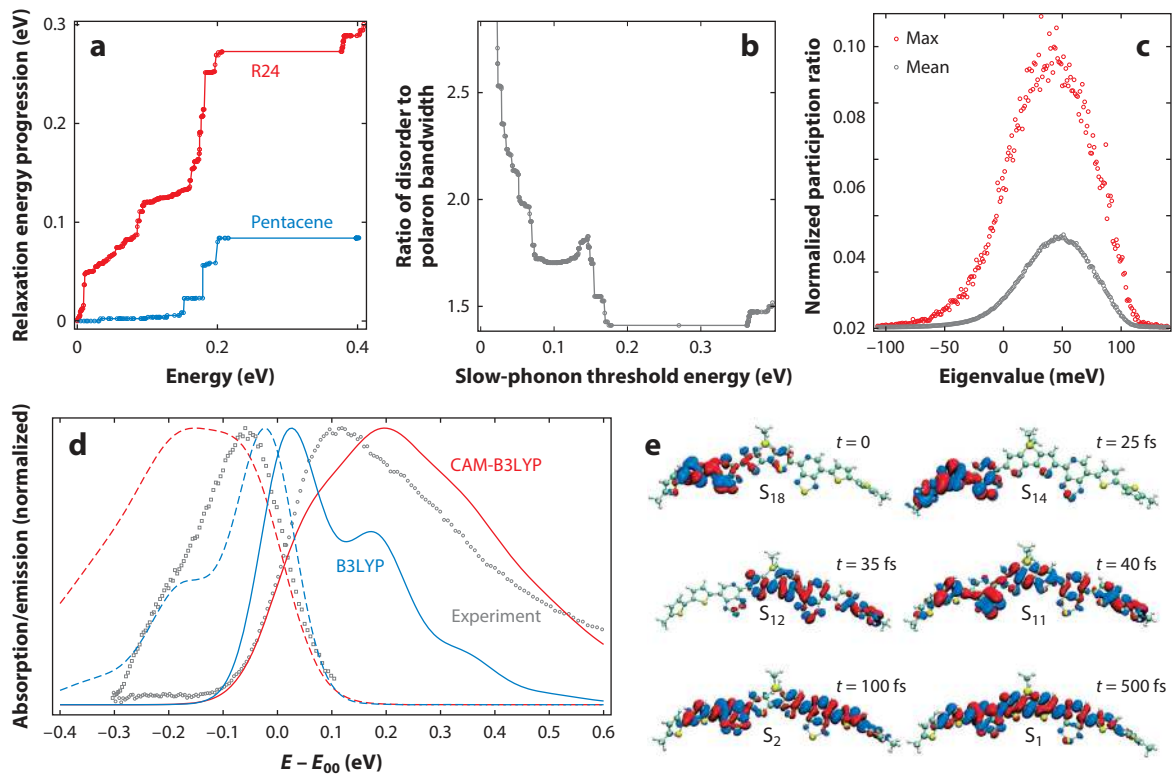


Figure 3

(a) Intramolecular relaxation energy progression of the hole polaron for the R24 and pentacene molecules. The small rigid pentacene molecule has fewer strongly coupled modes compared to the large and flexible R24 molecule, displaying a quasi-continuous distribution of coupling strength. (b) Ratio of disorder to polaron bandwidth for an R24 crystal. Independent of how modes are partitioned into fast and slow ones, the combined effect of static and dynamic disorder localizes excitons. (c) Localized excitons in an R24 crystal from the statistically sampled participation ratio (normalized to be 1 for a fully delocalized wave function; the supercell size is 20 nm or 5,000 molecules). (d) Absorption and emission spectra for the R24 molecule as calculated employing commonly used B3LYP and CAM-B3LYP functionals with a different amount of orbital exchange along with experimental data. (e) Nonradiative relaxation (internal conversion) from a high-energy absorption band to the lowest singlet excited state (S_1) in the R24 molecule, which involves multiple electronic states with different spatial extents of their wave functions. Panel *e* adapted with permission from Reference 18.

satisfy this condition. As a zero-point approximation, such modes can be considered as quasi-static disorder for intermolecular charge and energy transfer. Contrary to fast modes dynamically bound to excitons and charge carriers, slow modes are decoupled from the latter and localize them efficiently.

Generally, all three classes of strong electron-phonon interactions mentioned in the beginning of this section are important: The individual contributions of lattice and vibrational modes all together can cover the entire parameter space in **Figure 2b** just for one system. A representative distribution of local vibronic couplings is given by the R24 molecule in **Figure 3a**: A quasi-continuous distribution is observed with both slow and fast, and strongly and weakly coupled, modes. This fact severely complicates an accurate theoretical description of the electronic properties of such materials. In many situations, the overall coupling is strong enough to fully localize excitons and charge carriers. Such localization is not necessarily limited to a single monomer.

We illustrate the above speculations with two case studies: pentacene and R24. In rigid conjugated molecules, such as pentacene, the only strongly coupled vibrations are modes corresponding to C–C stretching (see **Figure 3a**). These modes just dress electronic states, without changing them substantially. The influence of lattice modes (six per molecule) is more intricate because of the low frequency, of the order of 10 meV for optical phonons (71, 77), and several complicating factors, such as mode mixing, anharmonism, and nonlinear coupling. For acenes at low-enough temperatures, of the order of 100 K, both first-principles (71, 86, 87) and experimental (32) investigations show a band-like electronic structure with a band shape very close to that without phonons (87), in agreement with MFP theory. Also in agreement with MFP theory is the temperature dependence of the band narrowing (88, 89). However, we are still lacking a rigorous experimental validation of first-principles calculations of electron-phonon effects. At room temperature, charge carriers may be dynamically localized in some acenes (71, 90).

In soft conjugated molecules, such as R24, there are many low-energy, strongly coupled intramolecular modes (see **Figure 3a**). Methods for an accurate solution of the Holstein Hamiltonian with such a broad distribution of ω_α and S_α are still lacking. Nevertheless, there is a simple, yet robust approach: We can divide all modes into fast and slow ones, consider the former as thermally averaged in the MFP method, and consider the latter as static disorder drawn from a thermal distribution. In particular, for excitons in an R24 crystal at 300 K, the disorder created by the frozen slow modes is always larger than the exciton bandwidth narrowed by the fast modes (**Figure 3b**), so that excitons in this system are localized (the result is independent of the fast/slow mode threshold). **Figure 3c** shows a typical distribution of the participation ratios: All states are localized; in particular, the thermally relaxed Frenkel excitons are localized on one monomer.

To summarize, a very approximate picture of electronic states in organic semiconductors emerges as follows: These states are polarons comprising C–C stretching modes, moving in a quasi-static disordered landscape created by thermal fluctuations of librational and lattice modes. A more accurate description requires an accurate modeling of electron-phonon correlations in the white region of the diagram in **Figure 2b**.

4.4. Ultraviolet-Visible and Ultraviolet Photoelectron Spectroscopies

The easiest direct test of an electron-phonon Hamiltonian is how accurately it can reproduce the shape of vibrationally resolved UV-Vis and ultraviolet photoelectron spectra (see also 91 for vibronic effects in the infrared spectra). In practice, quite often it is the only available efficient validation tool for theory. In particular, spectra of an ensemble of isolated molecules in vacuum or solution can be used to test local couplings obtained from first-principles calculations or to derive the parameters of the Holstein Hamiltonian from the experimentally measured spectra (for UV-Vis, see 20, 92–94; for ultraviolet photoelectron spectroscopy, see 95, 96). Importantly, the absorption and emission spectra of an isolated dipole-allowed electronic transition can be derived exactly within the Holstein Hamiltonian [independent boson or displaced oscillator model (63)] through the transition spectral density:

$$\sigma(E) = \sum_{nn'} \rho_n \langle n|n' \rangle \delta(E - E_{nn'}) \equiv \frac{1}{2\pi\hbar} \int_{-\infty}^{\infty} \hat{\sigma}(\tau) e^{i\tau E/\hbar} d\tau, \quad (9)$$

where ρ_n is the population of the initial vibrational state n , the prime denotes the final state of the transition, $\langle n|n' \rangle$ is the Franck–Condon factor, $E_{nn'}$ is the electronic plus vibrational transition energy, and $\hat{\sigma}(\tau)$ is the phonon correlator in the time domain, $\hat{\sigma}(\tau) = \langle e^{i\tau H_{\text{vib}}/\hbar} e^{-i\tau H'_{\text{vib}}/\hbar} \rangle$. For

the displaced oscillator model,

$$\hat{\sigma}(\tau) = \exp \left[\sum_{\alpha} S_{\alpha} \left(\coth \frac{\hbar\omega_{\alpha}}{2T} (\cos \omega_{\alpha} \tau - 1) - i \sin \omega_{\alpha} \tau \right) - i\omega_{00}\tau \right] \hat{\delta}(\tau), \quad (10)$$

where ω_{00} is the frequency of the 0-0 transition, and $\hat{\delta}$ is the Fourier transform of the lineshape function. The choice of the latter should not influence the result, especially for such large molecules as R24, whose low-frequency quasi-continuum of vibrational modes serves as a thermodynamic bath. **Figure 3d** shows simulated UV-Vis spectra for the R24 molecule in a solution. It is clearly seen that vibronic couplings are highly sensitive to the choice of the density functional. Vibronic mixing (the nontrivial Duschinsky matrix) is usually neglected for conjugated molecules (20, 92–94). However, there exists a generalization of Equation 10 for this case (97). Anharmonism may be important to explain the asymmetry between absorption and emission spectra (94).

Two important parameters can usually be robustly estimated from the experimental spectra of molecules in solution: the intramolecular polaron relaxation energy, λ , and vibrational bandwidth, W :

$$2\lambda = \bar{E}^{\text{absorption}} - \bar{E}^{\text{emission}} = 2 \sum_{\alpha} S_{\alpha} \hbar\omega_{\alpha}, \quad (11)$$

$$W^2 = \int \sigma(E)(E - \bar{E})^2 dE = \sum_{\alpha} S_{\alpha} \hbar^2 \omega_{\alpha}^2 \coth \frac{\hbar\omega_{\alpha}}{2T}, \quad (12)$$

where $\bar{E} = \int \sigma(E)E dE$.

For multimers and solids, the calculation of vibrationally resolved spectra is complicated (relative to the independent boson model) by the presence of closely spaced multiple excitations (see 17, figure 1) coupled through electron-phonon interaction. The most illustrative example is a symmetric dimer in an H- or J-aggregate configuration: One of the two excited states has a zero transition dipole in the equilibrium geometry of the dimer but quickly gains the dipole moment upon geometry fluctuations (the intermolecular Herzberg–Teller effect). Spectra in such cases can be evaluated by considering only strongly coupled quantum modes and only limited population of each of these modes (34). In particular, for dimers, the experimentally observed S_1/S_2 splitting follows the polaron renormalized intermolecular couplings given by Equation 8 (98). NAMD-based calculations of spectra can reproduce most of the spectral shape features, including vibrational broadening, Stokes shift, asymmetry between absorption and emission spectra, and Davydov splitting, but typically cannot address Franck–Condon progressions due to strongly coupled quantum modes.

4.5. Exciton and Charge Carrier Transport

Studies of energy and electron transfer in molecular systems have a long history (99). In most materials used in OPVs, the exciton and charge carrier transport proceeds through small polaron hopping. Although quantum correlations or coherences usually have minor effects in this process, there are strong classical correlations due to slow modes. NAMD can account for the latter, barring possible systematic errors in calculations of hopping probabilities. For the Holstein model in the MFP approximation, the hopping rates can be easily calculated using the perturbation theory over the intermolecular electronic couplings t (Fermi’s golden rule):

$$w = \frac{2\pi}{\hbar} |t|^2 K, \quad (13)$$

where K is the so-called spectral overlap:

$$K = \int \sigma_D(-E)\sigma_A(E) dE \equiv \frac{1}{2\pi\hbar} \int_{-\infty}^{\infty} \hat{\sigma}_D(\tau)\hat{\sigma}_A(\tau) d\tau, \quad (14)$$

where D/A represents the donor/acceptor. A simplified approach to account for nonlocal couplings is to replace $|t^2|$ by its average value (100). However, slow modes do not have time to equilibrate between hopping events (see Equation S7 in the **Supplemental Appendix**). The transport coefficients can then be calculated either by kinetic Monte Carlo simulations or by direct formulas. In the simplest case of a primitive lattice crystal, the diffusion tensor is given by $\mathbf{D} = (1/2) \sum_j w_{0j} \mathbf{r}_{0j} \otimes \mathbf{r}_{0j}$. The zero-field mobility can be obtained from \mathbf{D} by using the Einstein relationship $\mu T = eD$. For the general case, readers are referred to Reference 20.

Band-like transport is expected for pure crystals at low-enough temperatures. The MFP approximation can describe both hopping and band-like motion on the same footing (85). Here polaron and phonon Hamiltonians are separated. As a result, the formula for zero-field mobility is the same as for hopping but with a modified spectral overlap:

$$K = \frac{1}{2\pi\hbar} \int_{-\infty}^{\infty} \hat{\sigma}_D(\tau)\hat{\sigma}_A(\tau)\hat{\sigma}_{\text{polaron}}(\tau) d\tau, \quad (15)$$

where the polaron correlator in the case of a primitive lattice is given by (85)

$$\hat{\sigma}_{\text{polaron}}(\tau) = \frac{1}{N_{\text{cells}}} \sum_{k,k'} \rho(k) \exp \left[i \frac{\varepsilon(k) - \varepsilon(k')}{\hbar} \tau \right]. \quad (16)$$

Here $\varepsilon(k) = \sum_j t_{0j}^{\text{polaron}} e^{-ikr_{0j}}$ is polaron dispersion, and $\rho(k)$ is the normalized thermal population (usually Boltzmann distribution). Both $\hat{\sigma}_{\text{polaron}}(\tau)$ and $\hat{\sigma}_{\text{phonon}}(\tau) = \hat{\sigma}_D(\tau)\hat{\sigma}_A(\tau)$ at small τ decay as $\exp(-W^2\tau^2/2\hbar^2)$, where W is the corresponding bandwidth. The phonon bandwidth in the Holstein model is given by Equation 12. The polaron bandwidth is $W_{\text{polaron}}^2 = \langle \Delta\varepsilon \rangle^2 + \langle \Delta\varepsilon \rangle_T^2$, where the brackets with T represent the bandwidth of thermally populated states [weighted with $\rho(k)$]. Therefore, if $W_{\text{polaron}} \gg W_{\text{phonon}}$, then we have band-like transport. In the opposite case, we have small polaron hopping. Inhomogeneous broadening, scattering by static disorder, can be incorporated phenomenologically through the introduction of an empirical lineshape function $\hat{\delta}(\tau)$ into the integral in Equation 15 (e.g., the Gaussian function in 85).

An important conclusion of the MFP formula discussed above for zero-field mobility is that hopping models can be used far beyond their applicability (beyond the hopping regime) provided that the spectral overlap is properly rescaled to account for particle delocalization. In fact, on length scales larger than the scattering length, both the hopping and band models have the same diffusive limit (101). Moreover, in the case of narrow bands, $\hbar K$ can be interpreted as the polaron scattering time by comparing a mobility derived within the single scattering time approximation (102) with that obtained within the MFP approach.

5. ORGANIC SOLAR CELLS AND THEIR MODELING

As mentioned in Section 1, this review does not aim to provide comprehensive coverage of OPVs. Rather, it complements a set of largely nonoverlapping excellent reviews (2, 103–105) with an emphasis on recent progress.

An organic solar cell is a complex system with structural inhomogeneity on scales from tenths to hundreds of nanometers, involving physical processes on scales from femtoseconds to at least nanoseconds (see **Figure 1c**). A complete description of this system requires a multiscale modeling approach. A typical implementation of this approach in OPVs is as follows: On the scale of a few molecules, DFT is the best tool we currently have. To move to a larger scale, one can use a model

Hamiltonian, whose parameters are determined from DFT calculations. Next, for modeling of electronic processes in complex mesoscale structures, a master equation is appropriate, whose rates are determined through the model Hamiltonian. Usually, at this scale, the only way to obtain the geometry is via classical MD. Finally, at scales at which the microscopic details are completely washed out, continuum models can be applied.

There are a lot of studies investigating organic semiconductors and solar cells on each of these scales separately. The main challenge in first-principles multiscale modeling is to seamlessly combine different approaches on various scales (i.e., to perform coarse graining). Because a multitude of uncontrolled approximations are present at each scale, it is not easy to control the final accuracy of the calculated macroscopic quantities of interest. Presently, we have reliable schemes for two-scale modeling that allow for an evaluation of the exciton diffusion length and charge carrier mobility in bulk single-phase, chemically pure organic semiconductors. The next milestone, three-scale modeling, requires “molecule as a site” first-principles coarse graining. Such a routine is well established for large-scale MD and other simulations of structural properties (106). However, attempts to incorporate electronic processes have only recently been reported (107).

At the device scale, the methodological difference between organic and inorganic materials vanishes: The description is based on a diffusion equation for exciton or charge carrier transport and a Poisson equation for electrostatics. For this reason, we omit a discussion of this scale modeling and refer the readers to other works/reviews (3, 4, 103, 108).

5.1. Design of Organic Photovoltaic Materials

So far, the most successful and productive use of first-principles modeling in OPVs lies in the evaluation of structural and electronic properties of photovoltaic materials. The practical need requires not only the characterization of existing materials, but also the prediction of new ones. An illustrative example is the Harvard Clean Energy Project Database, containing two million candidate compounds for OPVs with calculated HOMO/LUMO energies (5). There are two basic approaches explored here: the analysis of intramolecular properties relying on the existence of structure-property relationships between single-molecule and bulk material properties and the direct modeling of the latter (e.g., the exciton diffusion length or charge carrier mobility).

The simplest, and very efficient, implementation of the first approach is to use HOMO/LUMO energies and the optical band gap of a molecular donor for the optimization of $\eta_{\text{abs}}(E_g)$ and V_{oc} of the device (1, 5). There are hundreds of compounds already synthesized with these two parameters nearly fully optimized. Thereby, the main efforts should now be put into improving J_{sc} and the fill factor, which strongly depends on the intermolecular and mesoscopic structure of the material. This calls for an experiment-based investigation of structure-property relationships between the chemical structure and macroscopic characteristics, with an emphasis on how small changes in the chemical composition can drive large changes in the physical properties of bulk materials (109, 110). Evidently, the molecular shape is an important factor influencing the intermolecular packing. Theoretical studies may help to uncover possible mechanisms of controlling the shape of flexible molecules by tuning the energetics of dihedral degrees of freedom (111).

The main challenge of bulk material modeling is the prediction of intermolecular packing. Even for molecular crystals, the intrinsic disorder, polymorphism, and dependence on the fabrication process severely complicate an accurate prediction of realistic structures (112). Modeling amorphous molecular and polymer solids is even more challenging. An instructive example comes from inorganic semiconductors: Amorphous silicon models correctly reproducing the structure factor have existed for decades, yet over all this time they have been improving in order to explain

a full set of experimental data (113). A stumbling block in the organic semiconductor realm is the strong dependence of charge carrier transfer rates on the intermolecular geometry. For these reasons, it is important to compare theoretical predictions with experimentally observed structures whenever possible (110, 114).


If the underlying structure is known, an evaluation of the exciton diffusion length and charge carrier mobility becomes a relatively routine procedure within the Holstein–Peierls Hamiltonian framework. As a result, the mechanisms and microscopic details of charge transport in organic semiconductors have been thoroughly investigated using first-principles modeling (20, 31, 64, 65, 102, 115–117). To discuss charge carrier (and exciton) mobility in molecular systems, we find it convenient to use an exact expression for the zero-field mobility with nearest-neighbor hopping on a primitive lattice (20):

$$\mu_0 = \frac{2\pi e}{\hbar} f a^2 t^2 \frac{K(T)}{T} \approx f \times (a[\text{\AA}] \cdot t)^2 \times \frac{K(T)}{T} \frac{\text{cm}^2}{\text{V} \cdot \text{s}}, \quad (17)$$

where f is the lattice form factor; a and t are the nearest-neighbor distance and electronic coupling, respectively; K is the spectral overlap; and T is the temperature. First-principles calculations allow us to evaluate all these parameters to understand the main factors influencing charge carrier mobility. In particular, the lattice form factor varies from 1 for π -stacks (e.g., R24), 3/2 for herringbone lattices (e.g., pentacene), and 2 for close packings (e.g., fullerene) to somewhat larger values for a long-range transfer (e.g., ~ 7 for excitons in R24). The hopping distance, a , can be as small as van der Waals distances (e.g., 3.5 Å for nonshifted π -stacks and 5 Å for close-packed herringbone lattices). Slip π -stacks and large molecules allow for larger values [e.g., 10 Å for a polymorph of R24 (110) and fullerene]. The polaron wave-function size sets the upper limit for a . Intermolecular couplings of the order of 100 meV are routinely reported for good organic semiconductors. The last factor, $K(T)/T$, is responsible for the temperature dependence and is the only factor evading an accurate description and thorough understanding. At room temperature, the hopping approximation is valid for most organic semiconductors, so Equation S4 in the **Supplemental Appendix** gives a rough upper limit for K . Assuming $W \sim 0.2$ eV and considering the values discussed above for the rest of the parameters, we end up with the charge carrier mobilities in the range 1–100 cm²/V/s for good organic semiconductors, which correspond to measured values. In other words, based on the current knowledge of conjugated molecules, there are no theoretical premises for small-molecule crystals to have mobilities much higher than 100 cm²/V/s.

For amorphous solids, K and t are effectively renormalized by on-site and off-diagonal disorder, respectively. As a result, macroscopic charge carrier mobilities in disordered, impure, and polycrystalline semiconductors are usually orders of magnitude smaller than those in the corresponding chemically pure single crystals, again in full accordance with observations. The situation with polymers is different: The intrinsic intrachain charge carrier mobility exceeds the observed bulk mobility by many orders of magnitude (102, 118). Therefore, with technological advances in obtaining better morphology of bulk polymer semiconductors, we may expect mobilities larger than those in small-molecule crystals (119). First-principles modeling of noncrystalline and impure organic semiconductors is still lacking robust quantitative accuracy, and empirical hopping models (120–122) remain very useful for the description of phenomena intrinsic to disordered systems, such as the Poole–Frenkel law for the field dependence of mobility (123).

A similar analysis can be performed for the exciton diffusion length. The calculated length exceeds 100 nm for perfect crystals (20, 124) and is reduced for disordered systems mainly by on-site energy variation (125). Experiments typically give substantially lower values (126, 127),

 **Supplemental Material**

implying that exciton diffusion is trap limited. This fact is consistent with the observation that the concentration of exciton quenchers (for amorphous solids) is nearly universal, approximately one trap per $(20 \text{ nm})^3$ (128). Consequently, this value roughly sets the limit for the maximum domain size in bulk heterojunction solar cells.

5.2. Organic-Organic Donor-Acceptor Interfaces

Electronic dynamics at heterojunction interfaces are critical for OPVs. Experimental and theoretical investigations of bulk heterojunctions are very limited because of the multiscale complexity of a real three-dimensional interface. Much simpler, although microscopically equivalent, is a planar donor-acceptor interface, allowing for full control and thorough analysis on the mesoscale at least. From a theoretical standpoint, such a one-dimensional inhomogeneity allows for a simplified formulation of atomistic (129) and continuum (108) models. In first-principles photovoltaic simulations, one needs to calculate the energies of CT states on an interface and to estimate the rates of two processes: CT state formation from an exciton that arrived at the interface by diffusion (exciton dissociation) and complete spatial separation of charges starting from that CT state (charge separation). These rates are to be compared with competing processes resulting in radiative or nonradiative electron-hole recombination (including triplet states). The generation of CT states directly through light absorption or by ultrafast relaxation from an excited state is possible (2) but not particularly efficient (130).

The main challenge for the atomistic modeling of interfaces is the same as for bulk materials: generating representative geometries (129). A macroscopically planar interface between two molecular crystals is not just a superposition of two crystals: Phase intermixing (131, 132) and molecular interdiffusion (133) are observed in MD simulations. In addition, electronic structure is sensitive to molecular orientation and thermal fluctuations. Therefore, calculated properties must be properly sampled statistically (129, 134, 135). The level of theory used in interface modeling varies from *ab initio* wave-function methods (136), NAMD (21, 137), and quantum dynamics (138) for model geometries to classical MD and simplified electronic Hamiltonians for statistically sampled simulations (134, 135, 139). Transfer integrals for exciton dissociation are usually evaluated as LUMO transfer integrals because all the LUMOs, anion natural orbitals, electron natural transition orbitals, and natural orbitals (singlet or triplet) have essentially the same spatial form of the wave function (see **Supplemental Figure 4**).

The results of calculations show that electronic properties for molecules at the interface differ from those in the bulk material because of geometry modulations by incommensurate lattices and the local electrostatic field by a built-in interfacial dipole (129, 140–142). The latter may induce bending of electronic levels of the order of tenths of an electron volt, extending to several nanometers in depth (141). The energy of CT states, E_{CT} , with respect to the bulk exciton, $E_{exc} \lesssim E_g$ (here the difference results from exciton relaxation), and the charge separated state, $E_{CS} \gtrsim eV_{oc}$ (here the difference results from generation-recombination balance), is crucial for photovoltaic performance. A high fill factor necessitates $E_{CT} \gtrsim E_{CS}$ to separate charges without an external field (130). In contrast to some inorganic interfaces in which E_{CT} is expected to be relevant to the HOMO/LUMO of the donor/acceptor, such a simple picture is hardly applicable to the OPV case due to strong Coulomb interactions, built-in electric fields, and other effects of the local environment. A high J_{sc} (low recombination) requires $E_{exc} - E_{CT} \gg T$ provided that the CT state itself does not have fast recombination channels. At the same time, $E_{exc} - E_{CT}$ must be low enough to have a high eV_{oc}/E_g ratio. The best trade-off value of $E_{exc} - E_{CT}$ has been found empirically to be a few tenths of an electron volt (1, 143). This value is similar to the

reorganization energy for an exciton-to-CT reaction, so the exciton dissociation proceeds resonantly in the Marcus formula (i.e., at the maximum possible rate) (see **Supplemental Figure 1**). The average electron transfer integrals are moderate (~ 10 meV) (134), but the resonance and multiple channels (especially into PCBM) make the exciton dissociation a very fast process (< 1 ps) (21). In contrast, charge separation is orders of magnitude slower (144). Three strategies are known to produce the required countergradient to overcome the strong long-range Coulomb attraction between an electron and a hole in low-dielectric constant materials and have $E_{CT} \gtrsim E_{CS}$ (140, 145, 146): an interfacial dipole, phase intermixing (147), and an entropic factor (148). Additionally, the introduction of a spacer layer between the donor and acceptor materials can significantly suppress recombination (149).

6. PERSPECTIVE

OPV technologies have come a long way due to groundbreaking advances in materials synthesis, experimental characterization, and theoretical modeling. Our progress in simulating organic semiconducting materials and electronic devices has reached the level of quantitative accuracy for ordered systems (single crystals, crystal-crystal interfaces). Similarly, first-principles modeling has become at least qualitative for disordered materials (thin films, bulk heterojunctions), and a detailed empirical description has emerged for device architectures (solar cells, light emitters). **Table 1** demonstrates that, compared to traditional photovoltaic technologies, further improvements in OPV most likely can be achieved with quantum efficiency (**Figure 1b**). This requires a fundamental understanding of various physical mechanisms leading to carrier losses and would particularly benefit from advanced theoretical simulations. Driven by this challenge, further progress is anticipated in extending multiscale modeling to larger scales (e.g., coarse graining to statistical hopping models) while improving the predictability of both first-principles and empirical approaches.

Advances in the underlying theoretical methodologies and the development of more efficient and flexible quantum-chemical and MD codes parallel to progress in computer technologies are important for the overall success of predictive materials design. In particular, more accurate density functional models for electronic structure calculations as well as force fields for structure and morphology prediction are being developed worldwide. Faster and more accurate NAMD approaches (e.g., correctly describing tunneling processes) are emerging. Nevertheless, accurate solvers of the Holstein–Peierls Hamiltonian for π -conjugated molecular systems have yet to be developed. Simulated amorphous and bulk heterojunction morphologies have yet to be thoroughly tested to determine if they are statistically equivalent to real materials. Many other technical challenges are discussed above.

On the way to the acceptance of OPV technologies, despite multiple technological and fundamental limitations, numerous electronic properties of organic semiconductors and devices remain far from their theoretical maxima, such as solar cell PCE, the conductivity of polymers, and the exciton diffusion length in crystals. Even though many structure-property relationships and design rules have already been established for OPV materials, in our modeling we have yet to obtain answers to a practically important question: What is the maximum PCE that can be achieved for a device based on a given molecule(s)?

DISCLOSURE STATEMENT

The authors are not aware of any affiliations, memberships, funding, or financial holdings that might be perceived as affecting the objectivity of this review.

ACKNOWLEDGMENTS

We thank K. Velizhanin and S. Athanasopoulos for useful discussions. We acknowledge the support of Laboratory Directed Research and Development (LDRD) funds, the Center for Integrated Nanotechnology (CINT), and the Center for Nonlinear Studies (CNLS) at Los Alamos National Laboratory (LANL). LANL is operated by Los Alamos National Security, LLC, for the National Nuclear Security Administration of the US Department of Energy under contract DE-AC52-06NA25396.

LITERATURE CITED

1. Scharber MC, Muhlbacher D, Koppe M, Denk P, Waldauf C, et al. 2006. Design rules for donors in bulk-heterojunction solar cells: towards 10% energy-conversion efficiency. *Adv. Mater.* 18:789–94
2. Heeger AJ. 2014. 25th anniversary article: Bulk heterojunction solar cells: understanding the mechanism of operation. *Adv. Mater.* 26:10–27
3. Koster LJA, Shaheen SE, Hummelen JC. 2012. Pathways to a new efficiency regime for organic solar cells. *Adv. Energy Mater.* 2:1246–53
4. Giebink NC, Wiederrecht GP, Wasielewski MR, Forrest SR. 2011. Thermodynamic efficiency limit of excitonic solar cells. *Phys. Rev. B* 83:195326
5. Hachmann J, Olivares-Amaya R, Atahan-Evrenk S, Amador-Bedolla C, Sánchez-Carrera RS, et al. 2011. The Harvard Clean Energy Project: large-scale computational screening and design of organic photovoltaics on the world community grid. *J. Phys. Chem. Lett.* 2:2241–51
6. Klauk H. 2012. *Organic Electronics II: More Materials and Applications*. New York: Wiley
7. Janssen RAJ, Nelson J. 2013. Factors limiting device efficiency in organic photovoltaics. *Adv. Mater.* 25:1847–58
8. Kanal IY, Owens SG, Bechtel JS, Hutchison GR. 2013. Efficient computational screening of organic polymer photovoltaics. *J. Phys. Chem. Lett.* 4:1613–24
9. Sumpter BG, Meunier V. 2012. Can computational approaches aid in untangling the inherent complexity of practical organic photovoltaic systems? *J. Polym. Sci. B* 50:1071–89
10. Servaites JD, Ratner MA, Marks TJ. 2011. Organic solar cells: a new look at traditional models. *Energy Environ. Sci.* 4:4410–22
11. Brédas JL, Norton JE, Cornil J, Coropceanu V. 2009. Molecular understanding of organic solar cells: the challenges. *Acc. Chem. Res.* 42:1691–99
12. Pope M, Swenberg C. 1999. *Electronic Processes in Organic Crystals and Polymers*. New York: Oxford Univ. Press
13. Sun Y, Welch GC, Leong WL, Takacs CJ, Bazan GC, Heeger AJ. 2012. Solution-processed small-molecule solar cells with 6.7% efficiency. *Nat. Mater.* 11:44–48
14. Beaujuge PM, Frechet JMJ. 2011. Molecular design and ordering effects in π -functional materials for transistor and solar cell applications. *J. Am. Chem. Soc.* 133:20009–29
15. Chen L, Furukawa K, Gao J, Nagai A, Nakamura T, et al. 2014. Photoelectric covalent organic frameworks: converting open lattices into ordered donor-acceptor heterojunctions. *J. Am. Chem. Soc.* 136:9806–9
16. Robb MJ, Ku S, Hawker CJ. 2013. No assembly required: recent advances in fully conjugated block copolymers. *Adv. Mater.* 25:5686–700
17. Bardeen CJ. 2014. The structure and dynamics of molecular excitons. *Annu. Rev. Phys. Chem.* 65:127–48
18. Oldani N, Tretiak S, Bazan G, Fernandez-Alberti S. 2014. Modeling of internal conversion in photoexcited conjugated molecular donors used in organic photovoltaics. *Energy Environ. Sci.* 7:1175–84
19. Clark J, Nelson T, Tretiak S, Cirmi G, Lanzani G. 2012. Femtosecond torsional relaxation. *Nat. Phys.* 8:225–31
20. Zhugayevych A, Postupna O, Bakus RC II, Welch GC, Bazan GC, Tretiak S. 2013. Ab initio study of a molecular crystal for photovoltaics: light absorption, exciton and charge carrier transport. *J. Phys. Chem. C* 117:4920–30

21. Jailaubekov AE, Willard AP, Tritsch JR, Chan WL, Sai N, et al. 2013. Hot charge-transfer excitons set the time limit for charge separation at donor/acceptor interfaces in organic photovoltaics. *Nat. Mater.* 12:66–73
22. Park SH, Roy A, Beaupré S, Cho S, Coates N, et al. 2009. Bulk heterojunction solar cells with internal quantum efficiency approaching 100%. *Nat. Photonics* 3:297–302
23. Kaake LG, Jasieniak JJ, Bakus RC, Welch GC, Moses D, et al. 2012. Photoinduced charge generation in a molecular bulk heterojunction material. *J. Am. Chem. Soc.* 134:19828–38
24. Devizis A, Meerholz K, Hertel D, Gulbinas V. 2010. Hierarchical charge carrier motion in conjugated polymers. *Chem. Phys. Lett.* 498:302–6
25. Koster LJA. 2010. Charge carrier mobility in disordered organic blends for photovoltaics. *Phys. Rev. B* 81:205318
26. Nayak PK, Cahen D. 2014. Updated assessment of possibilities and limits for solar cells. *Adv. Mater.* 26:1622–28
27. Schlenker CW, Thompson ME. 2011. The molecular nature of photovoltage losses in organic solar cells. *Chem. Commun.* 47:3702–16
28. Niv A, Gharghi M, Gladden C, Miller OD, Zhang X. 2012. Near-field electromagnetic theory for thin solar cells. *Phys. Rev. Lett.* 109:138701
29. Shockley W, Queisser HJ. 1961. Detailed balance limit of efficiency of *p-n* junction solar cells. *J. Appl. Phys.* 32:510–19
30. Chen K, Yip H, Salinas J, Xu Y, Chueh C, Jen A. 2014. Strong photocurrent enhancements in highly efficient flexible organic solar cells by adopting a microcavity configuration. *Adv. Mater.* 26:3349–54
31. Troisi A. 2011. Charge transport in high mobility molecular semiconductors: classical models and new theories. *Chem. Soc. Rev.* 40:2347–58
32. Ciuchi S, Hatch RC, Höchst H, Faber C, Blase X, Fratini S. 2012. Molecular fingerprints in the electronic properties of crystalline organic semiconductors: from experiment to theory. *Phys. Rev. Lett.* 108:256401
33. Cardona CM, Li W, Kaifer AE, Stockdale D, Bazan GC. 2011. Electrochemical considerations for determining absolute frontier orbital energy levels of conjugated polymers for solar cell applications. *Adv. Mater.* 23:2367–71
34. Spano FC. 2010. The spectral signatures of Frenkel polarons in H- and J-aggregates. *Acc. Chem. Res.* 43:429–39
35. Salaneck W, Friend R, Brédas J. 1999. Electronic structure of conjugated polymers: consequences of electron-lattice coupling. *Phys. Rep.* 319:231–51
36. Barford W. 2005. *Electronic and Optical Properties of Conjugated Polymers*. New York: Oxford Univ. Press
37. Brooks JS. 2008. Magnetic field dependent and induced ground states in organic conductors. *Rep. Prog. Phys.* 71:126501
38. Jacquemin D, Adamo C. 2011. Bond length alternation of conjugated oligomers: wave function and DFT benchmarks. *J. Chem. Theory Comput.* 7:369–76
39. Kozzardorfer T, Sears JS, Sutton C, Brédas JL. 2011. Long-range corrected hybrid functionals for π -conjugated systems: dependence of the range-separation parameter on conjugation length. *J. Chem. Phys.* 135:204107
40. Cramer C. 2005. *Essentials of Computational Chemistry: Theories and Models*. New York: Wiley
41. Magyar RJ, Tretiak S. 2007. Dependence of spurious charge-transfer excited states on orbital exchange in TDDFT: large molecules and clusters. *J. Chem. Theory Comput.* 3:976–87
42. Nayyar IH, Batista ER, Tretiak S, Saxena A, Smith DL, Martin RL. 2011. Localization of electronic excitations in conjugated polymers studied by DFT. *J. Phys. Chem. Lett.* 2:566–71
43. Burns LA, Vázquez-Mayagoitia A, Sumpter BG, Sherrill CD. 2011. Density-functional approaches to noncovalent interactions: a comparison of dispersion corrections (DFT-D), exchange-hole dipole moment (XDM), theory, and specialized functionals. *J. Chem. Phys.* 134:084107
44. Baer R, Livshits E, Salzner U. 2010. Tuned range-separated hybrids in density functional theory. *Annu. Rev. Phys. Chem.* 61:85–109
45. Mardirossian N, Head-Gordon M. 2014. Exploring the limit of accuracy for density functionals based on the generalized gradient approximation: local, global hybrid, and range-separated hybrid functionals with and without dispersion corrections. *J. Chem. Phys.* 140:18A527

46. Zhang CR, Sears JS, Yang B, Aziz SG, Coropceanu V, Brédas JL. 2014. Theoretical study of the local and charge-transfer excitations in model complexes of pentacene-C₆₀ using tuned range-separated hybrid functionals. *J. Chem. Theory Comput.* 10:2379–88
47. Autschbach J, Srebro M. 2014. Delocalization error and “functional tuning” in Kohn-Sham calculations of molecular properties. *Acc. Chem. Res.* 47:2592–602
48. Kubar T, Elstner M. 2010. Coarse-grained time-dependent density functional simulation of charge transfer in complex systems: application to hole transfer in DNA. *J. Phys. Chem. B* 114:11221–40
49. Bedard-Hearn MJ, Sterpone F, Rossky PJ. 2010. Nonadiabatic simulations of exciton dissociation in poly-*p*-phenylenevinylene oligomers. *J. Phys. Chem. A* 114:7661–70
50. Botelho AL, Shin Y, Liu J, Lin X. 2014. Structure and optical bandgap relationship of π -conjugated systems. *PLoS ONE* 9:e86370
51. Lukyanov A, Malafeev A, Ivanov V, Chen HL, Kremer K, Andrienko D. 2010. Solvated poly-(phenylene vinylene) derivatives: conformational structure and aggregation behavior. *J. Mater. Chem.* 20:10475–85
52. Zhang D, Qu Z, Liu C, Jiang Y. 2011. Excitation energy calculation of conjugated hydrocarbons: a new Pariser-Parr-Pople model parameterization approaching CASPT2 accuracy. *J. Chem. Phys.* 134:024114
53. Schapiro I, Ryazantsev MN, Frutos LM, Ferr N, Lindh R, Olivucci M. 2011. The ultrafast photoisomerizations of rhodopsin and bathorhodopsin are modulated by bond length alternation and HOOP driven electronic effects. *J. Am. Chem. Soc.* 133:3354–64
54. Coropceanu V, Sánchez-Carrera RS, Paramonov P, Day GM, Brédas JL. 2009. Interaction of charge carriers with lattice vibrations in organic molecular semiconductors: naphthalene as a case study. *J. Phys. Chem. C* 113:4679–86
55. Tully JC. 2012. Perspective: nonadiabatic dynamics theory. *J. Chem. Phys.* 137:22A301
56. Beck TL. 2000. Real-space mesh techniques in density-functional theory. *Rev. Mod. Phys.* 72:1041–80
57. Skouteris D, Barone V. 2014. A new Gaussian MCTDH program: implementation and validation on the levels of the water and glycine molecules. *J. Chem. Phys.* 140:244104
58. Nelson T, Fernandez-Alberti S, Roitberg AE, Tretiak S. 2014. Nonadiabatic excited-state molecular dynamics: modeling photophysics in organic conjugated materials. *Acc. Chem. Res.* 47:1155–64
59. Duncan WR, Prezhdov OV. 2007. Theoretical studies of photoinduced electron transfer in dye-sensitized TiO₂. *Annu. Rev. Phys. Chem.* 58:143–84
60. Martinelli NG, Ide J, Sánchez-Carrera RS, Coropceanu V, Brédas JL, et al. 2010. Influence of structural dynamics on polarization energies in anthracene single crystals. *J. Phys. Chem. C* 114:20678–85
61. Ben-Nun M, Quenneville J, Martínez TJ. 2000. Ab initio multiple spawning: photochemistry from first principles quantum molecular dynamics. *J. Phys. Chem. A* 104:5161–75
62. Shenvi N, Subotnik JE, Yang W. 2011. Simultaneous-trajectory surface hopping: a parameter-free algorithm for implementing decoherence in nonadiabatic dynamics. *J. Chem. Phys.* 134:144102
63. Mahan G. 2000. *Many-Particle Physics*. New York: Kluwer Acad.
64. Ortmann F, Bechstedt F, Hannewald K. 2011. Charge transport in organic crystals: theory and modelling. *Phys. Status Solidi B* 248:511–25
65. Coropceanu V, Cornil J, da Silva Filho DA, Olivier Y, Silbey R, Brédas JL. 2007. Charge transport in organic semiconductors. *Chem. Rev.* 107:926–52
66. Heeger AJ, Kivelson S, Schrieffer JR, Su WP. 1988. Solitons in conducting polymers. *Rev. Mod. Phys.* 60:781–850
67. Li H, Wu C, Malinin SV, Tretiak S, Chernyak VY. 2010. Excited states of donor and acceptor substituted conjugated oligomers: a perspective from the exciton scattering approach. *J. Phys. Chem. Lett.* 1:3396–400
68. Chowdary PD, Martínez TJ, Gruebele M. 2007. The vibrationally adiabatic torsional potential energy surface of *trans*-stilbene. *Chem. Phys. Lett.* 440:7–11
69. Papaconstantopoulos DA, Mehl MJ. 2003. The Slater-Koster tight-binding method: a computationally efficient and accurate approach. *J. Phys. Condens. Matter* 15:R413
70. Binder R, Romer S, Wahl J, Burghardt I. 2014. An analytic mapping of oligomer potential energy surfaces to an effective Frenkel model. *J. Chem. Phys.* 141:014101
71. Hannewald K, Stojanovic VM, Schellekens JMT, Bobbert PA, Kresse G, Hafner J. 2004. Theory of polaron bandwidth narrowing in organic molecular crystals. *Phys. Rev. B* 69:075211

72. Kirkpatrick J. 2008. An approximate method for calculating transfer integrals based on the ZINDO Hamiltonian. *Int. J. Quantum Chem.* 108:51–56
73. Hennebicq E, Pourtois G, Scholes GD, Herz LM, Russell DM, et al. 2005. Exciton migration in rigid-rod conjugated polymers: an improved Förster model. *J. Am. Chem. Soc.* 127:4744–62
74. Beljonne D, Curutchet C, Scholes GD, Silbey RJ. 2009. Beyond Förster resonance energy transfer in biological and nanoscale systems. *J. Phys. Chem. B* 113:6583–99
75. Huang J, Kertesz M. 2004. Intermolecular transfer integrals for organic molecular materials: Can basis set convergence be achieved? *Chem. Phys. Lett.* 390:110–15
76. Sutton C, Sears JS, Coropceanu V, Brédas JL. 2013. Understanding the density functional dependence of DFT-calculated electronic couplings in organic semiconductors. *J. Phys. Chem. Lett.* 4:919–24
77. Yi Y, Coropceanu V, Brédas JL. 2012. Nonlocal electron-phonon coupling in the pentacene crystal: beyond the Γ -point approximation. *J. Chem. Phys.* 137:164303
78. Moran D, Simmonett AC, Leach FE III, Allen WD, Schleyer P, Schaefer HF III. 2006. Popular theoretical methods predict benzene and arenes to be nonplanar. *J. Am. Chem. Soc.* 128:9342–43
79. Devreese JT, Alexandrov AS. 2009. Fröhlich polaron and bipolaron: recent developments. *Rep. Prog. Phys.* 72:066501
80. Wang L, Prezhdo OV. 2014. A simple solution to the trivial crossing problem in surface hopping. *J. Phys. Chem. Lett.* 5:713–19
81. Sterpone F, Martinazzo R, Panda AN, Burghardt I. 2011. Coherent excitation transfer driven by torsional dynamics: a model Hamiltonian for PPV type systems. *Z. Phys. Chem.* 225:541–51
82. Pereverzev A, Bittner ER. 2006. Time-convolutionless master equation for mesoscopic electron-phonon systems. *J. Chem. Phys.* 125:104906
83. Chen D, Ye J, Zhang H, Zhao Y. 2011. On the Munn-Silbey approach to polaron transport with off-diagonal coupling and temperature-dependent canonical transformations. *J. Phys. Chem. B* 115:5312–21
84. Thoss M, Wang H, Miller WH. 2001. Self-consistent hybrid approach for complex systems: application to the spin-boson model with Debye spectral density. *J. Chem. Phys.* 115:2991–3005
85. Ortmann F, Bechstedt F, Hannewald K. 2009. Theory of charge transport in organic crystals: beyond Holstein’s small-polaron model. *Phys. Rev. B* 79:235206
86. Vukmirovic N, Bruder C, Stojanovic VM. 2012. Electron-phonon coupling in crystalline organic semiconductors: microscopic evidence for nonpolaronic charge carriers. *Phys. Rev. Lett.* 109:126407
87. Cheng YC, Silbey RJ, da Silva Filho DA, Calbert JP, Cornil J, Brédas JL. 2003. Three-dimensional band structure and bandlike mobility in oligoacene single crystals: a theoretical investigation. *J. Chem. Phys.* 118:3764–74
88. Hatch RC, Huber DL, Höchst H. 2010. Electron-phonon coupling in crystalline pentacene films. *Phys. Rev. Lett.* 104:047601
89. Koch N, Vollmer A, Salzmann I, Nickel B, Weiss H, Rabe JP. 2006. Evidence for temperature-dependent electron band dispersion in pentacene. *Phys. Rev. Lett.* 96:156803
90. Troisi A, Orlandi G. 2006. Charge-transport regime of crystalline organic semiconductors: diffusion limited by thermal off-diagonal electronic disorder. *Phys. Rev. Lett.* 96:086601
91. Pochas CM, Spano FC. 2014. New insights on the nature of two-dimensional polarons in semiconducting polymers: infrared absorption in poly(3-hexylthiophene). *J. Chem. Phys.* 140:244902
92. Karabunarliev S, Baumgarten M, Bittner ER, Mullen K. 2000. Rigorous Franck–Condon absorption and emission spectra of conjugated oligomers from quantum chemistry. *J. Chem. Phys.* 113:11372–81
93. Dierksen M, Grimme S. 2004. The vibronic structure of electronic absorption spectra of large molecules: a time-dependent density functional study on the influence of “exact” Hartree-Fock exchange. *J. Phys. Chem. A* 108:10225–37
94. Heimel G, Daghofer M, Gierschner J, List EJW, Grimsdale AC, et al. 2005. Breakdown of the mirror image symmetry in the optical absorption/emission spectra of oligo(*para*-phenylene)s. *J. Chem. Phys.* 122:054501
95. Kera S, Yamane H, Ueno N. 2009. First-principles measurements of charge mobility in organic semiconductors: valence hole-vibration coupling in organic ultrathin films. *Prog. Surf. Sci.* 84:135–54

96. Coropceanu V, Gruhn NE, Barlow S, Lambert C, Durivage JC, et al. 2004. Electronic couplings in organic mixed-valence compounds: the contribution of photoelectron spectroscopy. *J. Am. Chem. Soc.* 126:2727–31
97. Velizhanin KA, Wang H. 2009. Dynamics of electron transfer reactions in the presence of mode mixing: comparison of a generalized master equation approach with the numerically exact simulation. *J. Chem. Phys.* 131:094109
98. Ottiger P, Leutwyler S, Koppel H. 2012. Vibrational quenching of excitonic splittings in H-bonded molecular dimers: The electronic Davydov splittings cannot match experiment. *J. Chem. Phys.* 136:174308
99. Nitzan A. 2006. *Chemical Dynamics in Condensed Phases*. New York: Oxford Univ. Press
100. Zhu L, Kim E, Yi Y, Ahmed E, Jenekhe SA, et al. 2010. Charge-transport properties of the tetraphenylbis(indolo[1,2-*a*])quinoline and 5,7-diphenylindolo[1,2-*a*]quinoline crystals. *J. Phys. Chem. C* 114:20401–9
101. Barford W, Duffy CDP. 2006. Role of quantum coherence and energetic disorder in exciton transport in polymer films. *Phys. Rev. B* 74:075207
102. Grozema FC, Siebbeles LDA. 2008. Mechanism of charge transport in self-organizing organic materials. *Int. Rev. Phys. Chem.* 27:87–138
103. Kippelen B, Brédas JL. 2009. Organic photovoltaics. *Energy Environ. Sci.* 2:251–61
104. Deibel C, Dyakonov V. 2010. Polymer–fullerene bulk heterojunction solar cells. *Rep. Prog. Phys.* 73:096401
105. Gaudiana R. 2012. Organic photovoltaics: challenges and opportunities. *J. Polym. Sci. B* 50:1014–17
106. Fritz D, Koschke K, Harmandaris VA, van der Vegt NFA, Kremer K. 2011. Multiscale modeling of soft matter: scaling of dynamics. *Phys. Chem. Chem. Phys.* 13:10412–20
107. Kordt P, Stenzel O, Baumeier B, Schmidt V, Andrienko D. 2014. Parametrization of extended Gaussian disorder models from microscopic charge transport simulations. *J. Chem. Theory Comput.* 10:2508–13
108. Liu F, Ruden PP, Campbell IH, Smith DL. 2012. Device model for electronic processes at organic/organic interfaces. *J. Appl. Phys.* 111:094507
109. Coughlin JE, Henson ZB, Welch GC, Bazan GC. 2014. Design and synthesis of molecular donors for solution-processed high-efficiency organic solar cells. *Acc. Chem. Res.* 47:257–70
110. van der Poll TS, Zhugayevych A, Chertkov E, Bakus RC II, Coughlin JE, et al. 2014. Polymorphism of crystalline molecular donors for solution-processed organic photovoltaics. *J. Phys. Chem. Lett.* 5:2700–4
111. Coughlin JE, Zhugayevych A, Bakus RC II, van der Poll TS, Welch GC, et al. 2014. A combined experimental and theoretical study of conformational preferences of molecular semiconductors. *J. Phys. Chem. C* 118:15610–23
112. Price SL. 2014. Predicting crystal structures of organic compounds. *Chem. Soc. Rev.* 43:2098–111
113. Drabold DA. 2011. Silicon: the gulf between crystalline and amorphous. *Phys. Status Solidi Rapid Res. Lett.* 5:359–60
114. Lukyanov A, Lennartz C, Andrienko D. 2009. Amorphous films of tris(8-hydroxyquinolinato)aluminium: force-field, morphology, and charge transport. *Phys. Status Solidi A* 206:2737–42
115. Andrienko D. 2015. Simulations of morphology and charge transport in supramolecular organic materials. In *Supramolecular Materials for Opto-Electronics*, ed. N Koch, HJ Schneider, M Shahinpoor, pp. 309–62. Cambridge, UK: R. Soc. Chem.
116. Brédas JL, Beljonne D, Coropceanu V, Cornil J. 2004. Charge-transfer and energy-transfer processes in π -conjugated oligomers and polymers: a molecular picture. *Chem. Rev.* 104:4971–5004
117. Shuai Z, Geng H, Xu W, Liao Y, André J. 2014. From charge transport parameters to charge mobility in organic semiconductors through multiscale simulation. *Chem. Soc. Rev.* 43:2662–79
118. Kaiser AB. 2001. Electronic transport properties of conducting polymers and carbon nanotubes. *Rep. Prog. Phys.* 64:1–49
119. Tseng HR, Phan H, Luo C, Wang M, Perez LA, et al. 2014. High-mobility field-effect transistors fabricated with macroscopic aligned semiconducting polymers. *Adv. Mater.* 26:2993–98
120. Fishchuk II, Kadashchuk A, Hoffmann ST, Athanasopoulos S, Genoe J, et al. 2013. Unified description for hopping transport in organic semiconductors including both energetic disorder and polaronic contributions. *Phys. Rev. B* 88:125202

121. Yu ZG, Smith DL, Saxena A, Martin RL, Bishop AR. 2001. Molecular geometry fluctuations and field-dependent mobility in conjugated polymers. *Phys. Rev. B* 63:085202
122. Walker AB, Kambili A, Martin SJ. 2002. Electrical transport modelling in organic electroluminescent devices. *J. Phys. Condens. Matter* 14:9825–76
123. Stallinga P. 2011. Electronic transport in organic materials: comparison of band theory with percolation/ (variable range) hopping theory. *Adv. Mater.* 23:3356–62
124. Tamura H, Matsuo Y. 2014. Exciton diffusion length and charge mobility in donor and acceptor materials in organic photovoltaics: tetrabenzoporphyrin and silylmethyl[60] fullerene. *Chem. Phys. Lett.* 598:81–85
125. Papadopoulos TA, Muccioli L, Athanasopoulos S, Walker AB, Zannoni C, Beljonne D. 2011. Does supramolecular ordering influence exciton transport in conjugated systems? Insight from atomistic simulations. *Chem. Sci.* 2:1025–32
126. Lunt RR, Benziger JB, Forrest SR. 2010. Relationship between crystalline order and exciton diffusion length in molecular organic semiconductors. *Adv. Mater.* 22:1233–36
127. Athanasopoulos S, Hennebicq E, Beljonne D, Walker AB. 2008. Trap limited exciton transport in conjugated polymers. *J. Phys. Chem. C* 112:11532–38
128. Mikhnenko OV, Kuik M, Lin J, van der Kaap N, Nguyen TQ, Blom PWM. 2014. Trap-limited exciton diffusion in organic semiconductors. *Adv. Mater.* 26:1912–17
129. Beljonne D, Cornil J, Muccioli L, Zannoni C, Brédas JL, Castet F. 2011. Electronic processes at organic-organic interfaces: insight from modeling and implications for opto-electronic devices. *Chem. Mater.* 23:591–95
130. Albrecht S, Vandewal K, Tumbleston JR, Fischer FSU, Douglas JD, et al. 2014. On the efficiency of charge transfer state splitting in polymer:fullerene solar cells. *Adv. Mater.* 26:2533–39
131. Fu Y, Risko C, Brédas JL. 2013. Intermixing at the pentacene–fullerene bilayer interface: a molecular dynamics study. *Adv. Mater.* 25:878–82
132. Miller NC, Cho E, Junk MJN, Gysel R, Risko C, et al. 2012. Use of X-ray diffraction, molecular simulations, and spectroscopy to determine the molecular packing in a polymer–fullerene bimolecular crystal. *Adv. Mater.* 24:6071–79
133. Treat ND, Brady MA, Smith G, Toney MF, Kramer EJ, et al. 2011. Interdiffusion of PCBM and P3HT reveals miscibility in a photovoltaically active blend. *Adv. Energy Mater.* 1:82–89
134. Fu YT, da Silva Filho DA, Sini G, Asiri AM, Aziz SG, et al. 2014. Structure and disorder in squaraine–C₆₀ organic solar cells: a theoretical description of molecular packing and electronic coupling at the donor–acceptor interface. *Adv. Funct. Mater.* 24:3790–98
135. D’Avino G, Mothy S, Muccioli L, Zannoni C, Wang L, et al. 2013. Energetics of electron–hole separation at P3HT/PCBM heterojunctions. *J. Phys. Chem. C* 117:12981–90
136. Borges I, Aquino AJA, Kohn A, Nieman R, Hase WL, et al. 2013. Ab initio modeling of excitonic and charge–transfer states in organic semiconductors: the PTB1/PCBM low band gap system. *J. Am. Chem. Soc.* 135:18252–55
137. Akimov AV, Prezhdo OV. 2014. Nonadiabatic dynamics of charge transfer and singlet fission at the pentacene/C₆₀ interface. *J. Am. Chem. Soc.* 136:1599–608
138. Burghardt I, Bittner ER, Tamura H, Pereverzev A, Ramon JGS. 2009. Ultrafast photophysics of organic semiconductor junctions. In *Energy Transfer Dynamics in Biomaterial Systems*, ed. I Burghardt, V May, DA Micha, ER Bittner, pp. 183–212. New York: Springer
139. Ide J, Mereau R, Ducasse L, Castet F, Bock H, et al. 2014. Charge dissociation at interfaces between discotic liquid crystals: the surprising role of column mismatch. *J. Am. Chem. Soc.* 136:2911–20
140. McMahan DP, Cheung DL, Troisi A. 2011. Why holes and electrons separate so well in polymer/fullerene photovoltaic cells. *J. Phys. Chem. Lett.* 2:2737–41
141. Cornil J, Verlaak S, Martinelli N, Mityashin A, Olivier Y, et al. 2013. Exploring the energy landscape of the charge transport levels in organic semiconductors at the molecular scale. *Acc. Chem. Res.* 46:434–43
142. Monti OLA, Steele MP. 2010. Influence of electrostatic fields on molecular electronic structure: insights for interfacial charge transfer. *Phys. Chem. Chem. Phys.* 12:12390–400
143. Few S, Frost JM, Kirkpatrick J, Nelson J. 2014. Influence of chemical structure on the charge transfer state spectrum of a polymer:fullerene complex. *J. Phys. Chem. Lett.* 118:8253–61

144. Rego LGC, Hames BC, Mazon KT, Joswig JO. 2014. Intramolecular polarization induces electron-hole charge separation in light-harvesting molecular triads. *J. Phys. Chem. C* 118:126–34
145. Nayak PK, Narasimhan KL, Cahen D. 2013. Separating charges at organic interfaces: effects of disorder, hot states, and electric field. *J. Phys. Chem. Lett.* 4:1707–17
146. Clarke TM, Durrant JR. 2010. Charge photogeneration in organic solar cells. *Chem. Rev.* 110:6736–67
147. Burke TM, McGehee MD. 2014. How high local charge carrier mobility and an energy cascade in a three-phase bulk heterojunction enable >90% quantum efficiency. *Adv. Mater.* 26:1923–28
148. Giazitzidis P, Argyrakis P, Bisquert J, Vikhrenko VS. 2014. Charge separation in organic photovoltaic cells. *Org. Electron.* 15:1043–49
149. Nie W, Gupta G, Crone BK, Liu F, Smith DL, et al. 2014. Interface design principles for high efficiency organic semiconductor devices. Manuscript under review
150. Barišić OS, Barišić S. 2008. Phase diagram of the Holstein polaron in one dimension. *Eur. Phys. J. B* 64:1–18
151. Green MA, Emery K, Hishikawa Y, Warta W, Dunlop ED. 2013. Solar cell efficiency tables (version 41). *Prog. Photovolt. Res. Appl.* 21:1–11
152. Lunt RR, Osedach TP, Brown PR, Rowehl JA, Bulovic V. 2011. Practical roadmap and limits to nano-structured photovoltaics. *Adv. Mater.* 23:5712–27



Contents

Molecules in Motion: Chemical Reaction and Allied Dynamics in Solution and Elsewhere <i>James T. Hynes</i>	1
Crystal Structure and Prediction <i>Tejender S. Thakur, Ritesh Dubey, and Gautam R. Desiraju</i>	21
Reaction Dynamics in Astrochemistry: Low-Temperature Pathways to Polycyclic Aromatic Hydrocarbons in the Interstellar Medium <i>Ralf I. Kaiser, Dorian S.N. Parker, and Alexander M. Mebel</i>	43
Coherence in Energy Transfer and Photosynthesis <i>Aurélia Chenu and Gregory D. Scholes</i>	69
Ultrafast Dynamics of Electrons in Ammonia <i>Peter Vöhringer</i>	97
Dynamics of Bimolecular Reactions in Solution <i>Andrew J. Orr-Ewing</i>	119
The Statistical Mechanics of Dynamic Pathways to Self-Assembly <i>Stephen Whitelam and Robert L. Jack</i>	143
Reaction Dynamics at Liquid Interfaces <i>Ilan Benjamin</i>	165
Quantitative Sum-Frequency Generation Vibrational Spectroscopy of Molecular Surfaces and Interfaces: Lineshape, Polarization, and Orientation <i>Hong-Fei Wang, Luis Velarde, Wei Gan, and Li Fu</i>	189
Mechanisms of Virus Assembly <i>Jason D. Perlmutter and Michael F. Hagan</i>	217
Cold and Controlled Molecular Beams: Production and Applications <i>Justin Jankunas and Andreas Osterwalder</i>	241
Spintronics and Chirality: Spin Selectivity in Electron Transport Through Chiral Molecules <i>Ron Naaman and David H. Waldeck</i>	263

DFT: A Theory Full of Holes? <i>Aurora Pribram-Jones, David A. Gross, and Kieron Burke</i>	283
Theoretical Description of Structural and Electronic Properties of Organic Photovoltaic Materials <i>Andriy Zhubayevych and Sergei Tretiak</i>	305
Advanced Physical Chemistry of Carbon Nanotubes <i>Jun Li and Gai P. Pandey</i>	331
Site-Specific Infrared Probes of Proteins <i>Jianqiang Ma, Ileana M. Pazos, Wenkai Zhang, Robert M. Culik, and Feng Gai</i>	357
Biomolecular Damage Induced by Ionizing Radiation: The Direct and Indirect Effects of Low-Energy Electrons on DNA <i>Elabe Alizadeh, Thomas M. Orlando, and Léon Sanche</i>	379
The Dynamics of Molecular Interactions and Chemical Reactions at Metal Surfaces: Testing the Foundations of Theory <i>Kai Golibrzuch, Nils Bartels, Daniel J. Auerbach, and Alec M. Wodtke</i>	399
Molecular Force Spectroscopy on Cells <i>Baoyu Liu, Wei Chen, and Cheng Zhu</i>	427
Mass Spectrometry of Protein Complexes: From Origins to Applications <i>Shahid Mehmood, Timothy M. Allison, and Carol V. Robinson</i>	453
Low-Temperature Kinetics and Dynamics with Coulomb Crystals <i>Brianna R. Heazlewood and Timothy P. Softley</i>	475
Early Events of DNA Photodamage <i>Wolfgang J. Schreier, Peter Gilch, and Wolfgang Zinth</i>	497
Physical Chemistry of Nanomedicine: Understanding the Complex Behaviors of Nanoparticles in Vivo <i>Lucas A. Lane, Ximei Qian, Andrew M. Smith, and Shuming Nie</i>	521
Time-Domain Ab Initio Modeling of Photoinduced Dynamics at Nanoscale Interfaces <i>Linjun Wang, Run Long, and Oleg V. Prezhdo</i>	549
Toward Design Rules of Directional Janus Colloidal Assembly <i>Jie Zhang, Erik Luijten, and Steve Granick</i>	581
Charge Transfer-Mediated Singlet Fission <i>N. Monahan and X.-Y. Zhu</i>	601
Upconversion of Rare Earth Nanomaterials <i>Ling-Dong Sun, Hao Dong, Pei-Zhi Zhang, and Chun-Hua Yan</i>	619

Computational Studies of Protein Aggregation: Methods and Applications <i>Alex Morriss-Andrews and Joan-Emma Shea</i>	643
Experimental Implementations of Two-Dimensional Fourier Transform Electronic Spectroscopy <i>Franklin D. Fuller and Jennifer P. Ogilvie</i>	667
Electron Transfer Mechanisms of DNA Repair by Photolyase <i>Dongping Zhong</i>	691
Vibrational Energy Transport in Molecules Studied by Relaxation-Assisted Two-Dimensional Infrared Spectroscopy <i>Natalia I. Rubtsova and Igor V. Rubtsov</i>	717

Indexes

Cumulative Index of Contributing Authors, Volumes 62–66	739
Cumulative Index of Article Titles, Volumes 62–66	743

Errata

An online log of corrections to *Annual Review of Physical Chemistry* articles may be found at <http://www.annualreviews.org/errata/physchem>